

## Abstract

This research aims to develop a more complete model of how the Central Graben, which is located in the North Sea, formed as a result of overprinting of Paleozoic and Mesozoic tectonics. The first interpretations of Paleozoic stratigraphy and structures under the CG are shown. The Central graben is a passive rift, meaning extension took place through mechanical stretching rather than volcanic activity driving the extension. The earliest structures influencing the formation of the Central Graben formed during the Paleozoic and are likely related to Caledonian structures. Thus it is important to incorporate the Paleozoic grain in the subsequent tectonic events. The most important phases of rifting forming the CG occurred in the Mesozoic. Cretaceous and Cenozoic inversion phases caused reactivation of older faults. During all these different phases of deformation halokinesis of Zechstein salts also had a major effect on the formation of the Central Graben as it is observed today.

Most reconstructions or models do not account for the structures located below the Zechstein evaporites, as the thick sequence of salt makes imaging of these structures difficult. However, recent data acquisitions have made these structures more clear, allowing for a more accurate interpretation of the deeper structures. These sub-salt structures are kinematically linked with structures observed in the supra-salt sediments. They are thus of importance when studying the basin development. This research shows the first interpretations on the Paleozoic units and structures under the CG.

This research may aid in the further understanding of the effects of pre-existing crustal structures on the evolution of salt-influenced rifts. An application of this study is that earlier unrecognized hydrocarbon migration paths or trapping structures could be identified with these findings. Existing burial graphs, extension velocity models or calculated sedimentation rates may be reviewed with the results of this research in future work.

This research finds that large basement faults within the Paleozoic units and the detachment between Avalonia and Baltica have been of major importance for the formation of the Central Graben. After the Caledonian Orogeny finished, the accretionary complex collapsed, separating Avalonia and Baltica. The old suture between these 2 paleocontinents is currently recognized as the Thor Suture Zone. As the detachment weakened the crust strain localisation occurred, reactivating basement faults during later tectonic phases. This shows the it is fundamental to study basement structures when studying basin formation. Salt layers prevented the faults from propagating into the supra-salt cover. The CG is thus an asymmetric soft-linked half-graben.

# Using interplay of sub- and supra salt structures for an extensive formation model of the Central Graben, North Sea

L.H.J. Eskens

July 29, 2020

## 1 Introduction

The Central Graben (CG) is located in the central part of the North Sea (NS) (see Figure 1 for the exact location) and is part of the intracontinental Central European Basin System (CEBS). In this system Paleozoic and Mesozoic basins such as the CG formed. The CG is part of the Mesozoic rift system which consists of 3 different arms [Ziegler (1990b)], including the Central Graben, the Viking Graben and the Moray Firth Basin (See Figure 1 for exact locations). The deepest part of the CG, i.e. where the Base Zechstein is at its deepest, lies in the northern part of the CG. This directly overlies the assumed position of the Baltica margin by Smit et al. (2018). The CG overlies the collapsed accretionary complex and margin of Baltica (Figure 1).

The CG formed as the result of subsequent tectonic events during the Paleozoic and Mesozoic, each event influencing the localisation of deformation and thus the structure of the basin [Ziegler (1990a)]. The overprinting of different regional tectonic events is important to understand the formation of the CG. The graben has extensively been studied by both academics to study salt-influenced rift basins as well as the exploration industry in the search for hydrocarbons [e.g. Ziegler (1992), De Jager (2003), van Winden et al. (2018), ter Borgh et al. (2019), Doornenbal and Stevenson (2010)]. Besides regional tectonic events, halokinesis has been a very important mechanism in the formation of the basin as observed today as well [Ziegler (1982b), Van Wijhe (1987)].

The thick Zechstein salt layer deposited in the Late Permian separates the Mesozoic cover from Paleozoic basement [Ziegler (1990a)]. Both the Mesozoic cover sediments and the Paleozoic basement show corresponding extensional kinematics, being roughly E-W directed [Ziegler (1990b), Lundmark et al. (2012)]. However where Zechstein salt is of sufficient thickness, structural styles of these two different sequences differ [Nalpas et al. (1995)]. Because evaporites are generally weaker than surrounding sediments, salt sequences often localize strain and inhibit the upward propagation of faults rooted in the sub-salt sequence [Nalpas et al. (1995)]. This leads to thin-skinned tectonics in the supra-salt sequence, resulting in different structural styles between sub-and supra salt layers. Earlier formed salt structures also influence the deformation during later phases of tectonic activity [Van Wijhe (1987), Jackson and Vendeville (1994)].

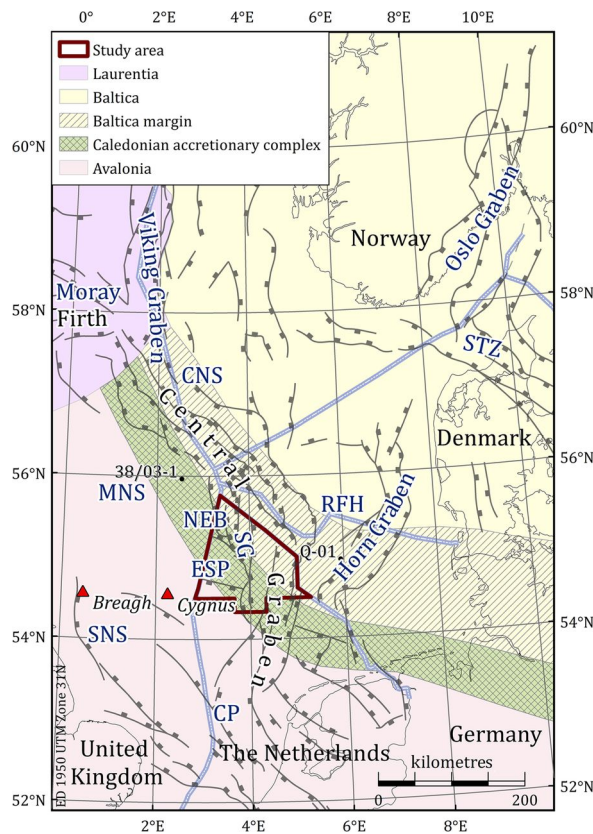


Figure 1: Map showing the regional overview of the study area and large-scale structures. Central North Sea (CNS), Cleaver Bank Platform (CP), Elbow Spit Platform (ESP), Mid North Sea High (MNS), North Elbow Basin (NEB), Step Graben (SG), Southern North Sea (SNS), Sorgenfrei-Tornquist Zone (STZ), Ringkøbing-Fyn High (RFH). Source: ter Borgh et al. (2019).

Many studies on the Central Graben do not take the Paleozoic basement structures into account when making reconstructions or models [e.g. van Winden et al. (2018)]. Subsalt imaging is difficult because of the wave energy loss during acquisition when thick layers of salt are present, as in some areas the Zechstein salt may reach a thickness of up to 1500m [Ziegler (1990a)]. Because of this thick Zechstein layer only poor quality seismic sections of the Paleozoic structures have been available, which makes it difficult to interpret the Paleozoic structures and relate them with the overlying structures. The Paleozoic sequence contains reactivated faults accommodating Mesozoic extension related to the formation of the Mesozoic basins however [Smit et al. (2018)], influencing the basin development. Therefore these deep structures need to be taken into account when the formation of the CG is studied. Overprinting of Paleozoic and Mesozoic faults and corresponding basins can be observed in the NS region (Figure 2). It stresses the importance of the Paleozoic structures in the localisation of displacement during subsequent tectonic events. Boundaries between different crustal terranes can be linked to zones of repeated deformation in the upper crust, which is a relation observed at the CG as well [Smit et al. (2018)].

Modern seismic data sets show the Paleozoic sub-salt sequence in more detail as salt penetration increased in more modern data acquisitions of the North Sea Renaissance project [Jansen et al. (2016)]. With this new data set we can get a better understanding of the Paleozoic basement structures. Combining these Paleozoic structures with the well studied geological history of the NS can help in finding a relation between the Paleozoic and

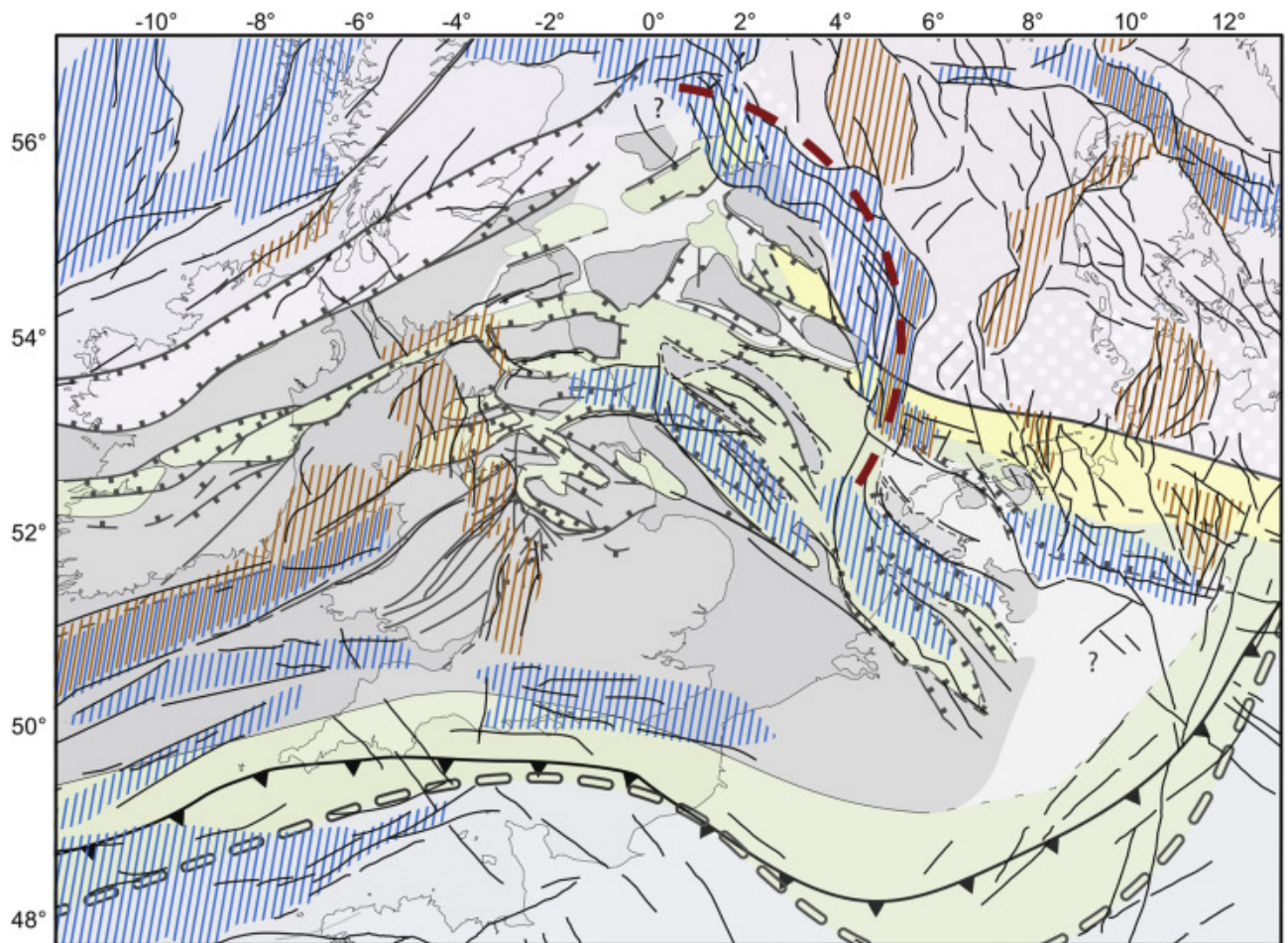


Figure 2: Comparison of Paleozoic and Mesozoic overprinting of fault networks and fault-bounded basins in northwestern Europe. This figure shows the importance of earlier formed structures on the location of subsequent basin forming processes. Black lines are Mesozoic faults, brown hatching is Permo-Triassic fault-bounded basin, blue hatching is Jurassic fault-bounded basin, red dotted line is Variscan proto-Central Graben. Source: Smit et al. (2018).

Mesozoic tectonic events. The objective of this research is to study the role of deeper, upper crustal structures in the development of the CG. The result of this research may act as the base for a future restoration of the CG and help shed light on the formation of the CG as well as salt-influenced rifts in general.

In summary this research will use modern seismic data and anomaly field data which allows for the Paleozoic structures underneath the Zechstein evaporites to be observed. These observed structures in the Paleozoic sequence are interpreted and used in combination with Mesozoic cover structures to obtain a more accurate model of formation for the CG. This model may serve as a base for a more complete reconstruction.

## 2 Structural framework of the southern North Sea

The southern North Sea is formed by different terranes which collided with one another through the Late Ordovician - Silurian to Early Devonian [Ziegler (1990a)]. Figure 3 shows these different terranes and their presumed locations. During the breakup of Pangea global extensional kinematics defined the tectonic setting. In the NS area old sutures of different lithospheric compositions and thicknesses allowed for the localisation of

strain. This is evidenced by the superposition of structures formed during different tectonic events [Færseth (1996)].

The 2 main events leading to the different phases of extension and inversion which formed the CG are (1) the break-up of Pangea due to rifting and (2) the closure of the Tethys Ocean due to Alpine collision [Ziegler (1990b)]. In the Paleozoic different extensional events during the Devonian and Carboniferous formed the first faults playing a key role in the formation of the CG. It is debated whether the basin that formed during the Paleozoic could be a proto-Central Graben [Ziegler (1990b)], with the Paleozoic structures affecting the formation of Mesozoic basins. The Mesozoic SG and CG are characterized by roughly N-S trending faults, while the proto-Central Graben is formed along 040°N structures [ter Borgh et al. (2019)]. Reactivation of these Paleozoic faults during the Mesozoic tectonic events was of major importance during the development of the CG.

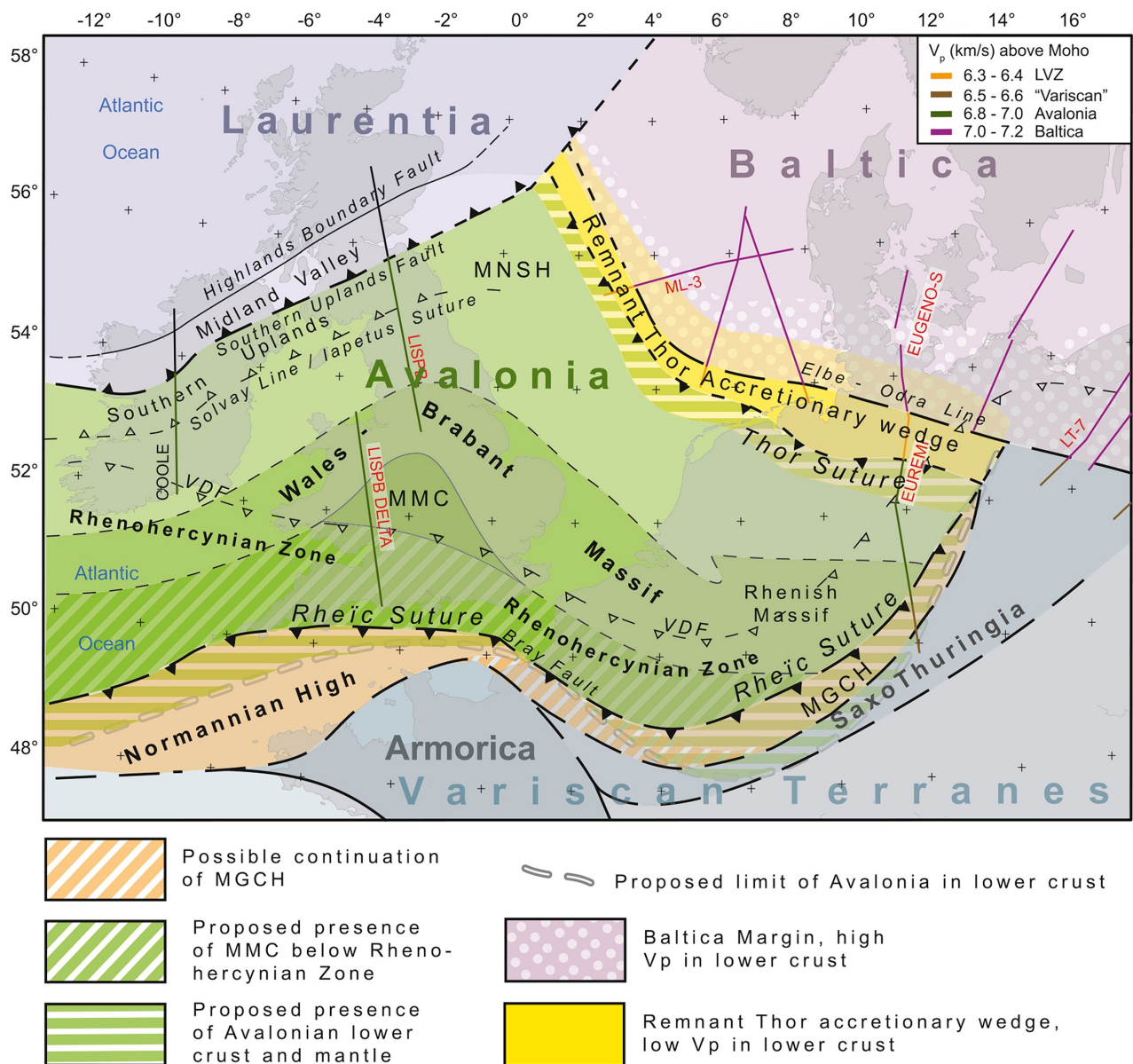


Figure 3: This figure shows the different terranes underlying the rift system of the North Sea. These different terranes cause weakening of the crust which may have localised the rifting in the North Sea. Source: Smit et al. (2018)

Throughout the Mesozoic multiple pulses of rifting occurred, followed by inversion at the end of the Cretaceous and continuing the Cenozoic [Ziegler (1990a)]. The CG is a perfect example of a multi-phase rift, where faults with different orientations interacting with one another are observed [Duffy et al. (2015)]. Combined with pre-existing Devonian and Carboniferous faults the Mesozoic tectonic phases resulted in a complex geology [Lyngsie and Thybo (2007)], paired with extensive salt tectonics of the Permian Zechstein evaporites [Van Wijhe (1987), Ziegler (1990a)]. The halokinesis caused subsidence where salt withdrew and uplift where it accumulated into salt walls and diapirs. These salt movements caused creation of paleotopographic features, influencing the depositional style. These salt structures sometimes formed local depocenters, influencing the depositional pattern of syn-kinematic sediments [Karlo et al. (2014)].

## 2.1 Cambro-Silurian

Avalonia, one of the peri-Gondwana terranes, was a passive margin of Gondwana [Torsvik and Cocks (2013)]. The Early Paleozoic history of Avalonia separating from Gondwana has been summarised in multiple previous works [e.g. Ziegler (1990a), Cocks and Fortey (2009), Matthews et al. (2016)]. During the Cambro-Ordovician period Avalonia started rifting from Gondwana and drifted to the north towards Baltica. Due to this northward drift the Thor Ocean was closed around the Late Ordovician-Silurian. When colliding, Baltica underthrust Avalonia towards the southwest, forming the Thor Suture Zone (TSZ) and Caledonian orogen in the process. The evolution of the foreland basins of the Caledonian orogen from the northwest towards the southeast indicated that the collision was oblique and occurred in a zipper-like way [Ziegler (1990a), Mazur et al. (2015)]. The Upper Paleozoic units sediments incorporated in the thrust wedge represent Caledonian low-grade metamorphosed shelf slope sediments [Berthelsen (1992)]. These Upper Paleozoic sediments were overthrust over Cambro-Silurian passive margin deposits of Baltica as continental collision occurred.

These collapsed Caledonian accretions now separate Avalonia and Baltica, indicated by a LVZ accretionary wedge [Smit et al. (2016)]. At the same time the Tornquist Sea subducted southward underneath as Avalonia and Laurentia collided. This is indicated by volcanic rocks [e.g. Woodcock (2012), Verniers et al. (2002)]. The LISP profiles show that the Avalonian crust is divided into 2 different velocity layers with velocities of 6.6 and  $6.9 \frac{km}{s}$  [Smit et al. (2018)]. When the Thor Ocean was completely closed the subduction from the Tornquist Sea flipped from southward underneath Avalonia to northward under Laurentia, as Avalonia "soft docked", meaning the collision wasn't paired with a lot of magmatism or deformation [Torsvik and Rehnström (2003)]. The forming of these two sutures called the Thor suture and Iapetus suture were part of the Caledonian Orogeny and formed the continent of Laurussia [Ziegler (2012)].

## 2.2 Devonian - Early Carboniferous

In the Early Devonian the final activity of the Caledonian orogen ceased and subduction ended, likely with slab break off of the Baltic slab [Mazur et al. (2018)]. South of the study area of this research another important

tectonic phase occurred. In the Early Devonian Gondwana followed Avalonia northward due to the closing of the Rheic Ocean. Northward subduction of Gondwana under Avalonia occurred as the Rheic Ocean completely closed and formed the Rheic Suture, forming Pangea as a result [Ballèvre et al. (2009), Winchester et al. (2002)]. After subduction stopped the Variscan Orogeny was initiated in the Late Devonian [Ziegler (1990a)].

Extension of the Avalonia microplate followed in the Late Devonian to Early Carboniferous, forming Early Carboniferous basins with a NE-SW orientation [Smit et al. (2018)]. Lundmark et al. (2012) find Famennian (Late Devonian) volcanics in well A17-01 (Figure 6 for exact location) on the northern flank of the ESP, which they attribute to either east-west extension or strike-slip tectonics during the Late Devonian. Well E06-01 (Figure 6 for exact location) shows intrusives within the Farne group (NAM drilling report E06-01). The finding of these volcanics suggests that volcanic activity continued throughout the Early Carboniferous. The extension causing volcanic activity would have formed a narrow Middle Devonian seaway [Ziegler (1990b)]. Recent studies [ter Borgh et al. (2019)] suggested there wasn't a narrow seaway, but rather a larger part of the study area was flooded in the Middle Devonian. Van Wees et al. (2000) and Neumann et al. (2004) find that the volcanics during the Carboniferous-Permian transition are related to extensive tectonics. These volcanics are likely related to plume activity of the Skagerrak-Centered Large Igenous Province (SCLIP) [Torsvik et al. (2008)]. The magmas formed due to plume activity at the base of the lithosphere. The magmas then travel up-slope to a thinned part of the lithosphere where they can erupt [Sleep (1997), Sleep (2006)]. The formation of the Southern Permian Basin (SPB) and Northern Permian Basin (NPB) also started as a result of this extension. These basins further developed as a result of thermal subsidence after a period of extensional tectonics during the Early Carboniferous and volcanic activity in the Early Permian [Coward (1995), Coward et al. (2003)]. The Variscan Orogeny changed the mainly extensional motion paired with subsidence in the Devonian and Early Carboniferous to strike-slip in the Late Carboniferous to Early Perm in the southern North Sea along NW-SE trending faults [Abramovitz et al. (1997), Coward et al. (2003)].

### **2.3 Late Carboniferous - Early Perm**

During the Late Carboniferous inversion of the southern North Sea took place due to the Variscan Orogeny [Coward et al. (2003)]. During this period the Mid North Sea High (MNSH) was uplifted [Ziegler (1990a), Coward et al. (2003)], which would then form the separation between the Northern and Southern Permian basins. The convergent motion of the Variscan Orogeny ended in the Westphalian in the Late Carboniferous and inversion ceased [Ziegler (1990a)]. The inversion due to the Variscan Orogeny was followed by volcanic activity and crustal thinning during the Carboniferous-Perm transition [Neumann et al. (2004), Van Wees et al. (2000)]. These volcanics resulted from the activity of the SCLIP [Torsvik et al. (2008)]. This magmatism caused thermal uplift of the Southern North Sea in the Early Perm [Ziegler (1990a)].

Figure 4 shows the locations of both the NPB and SPB in the Early Permian. A period without tectonic activity is assumed during the Early Permian, as the Rotliegend sandstones seem to have been deposited without

any tectonic influence [Ziegler (1992), Coward et al. (2003)]. The Caledonian mountain range towards the north acted as a sediment source for the northern basin while the Variscan mountain range towards the south acted as a sediment source for the southern basin [Ziegler (1988), Glennie (1984)].

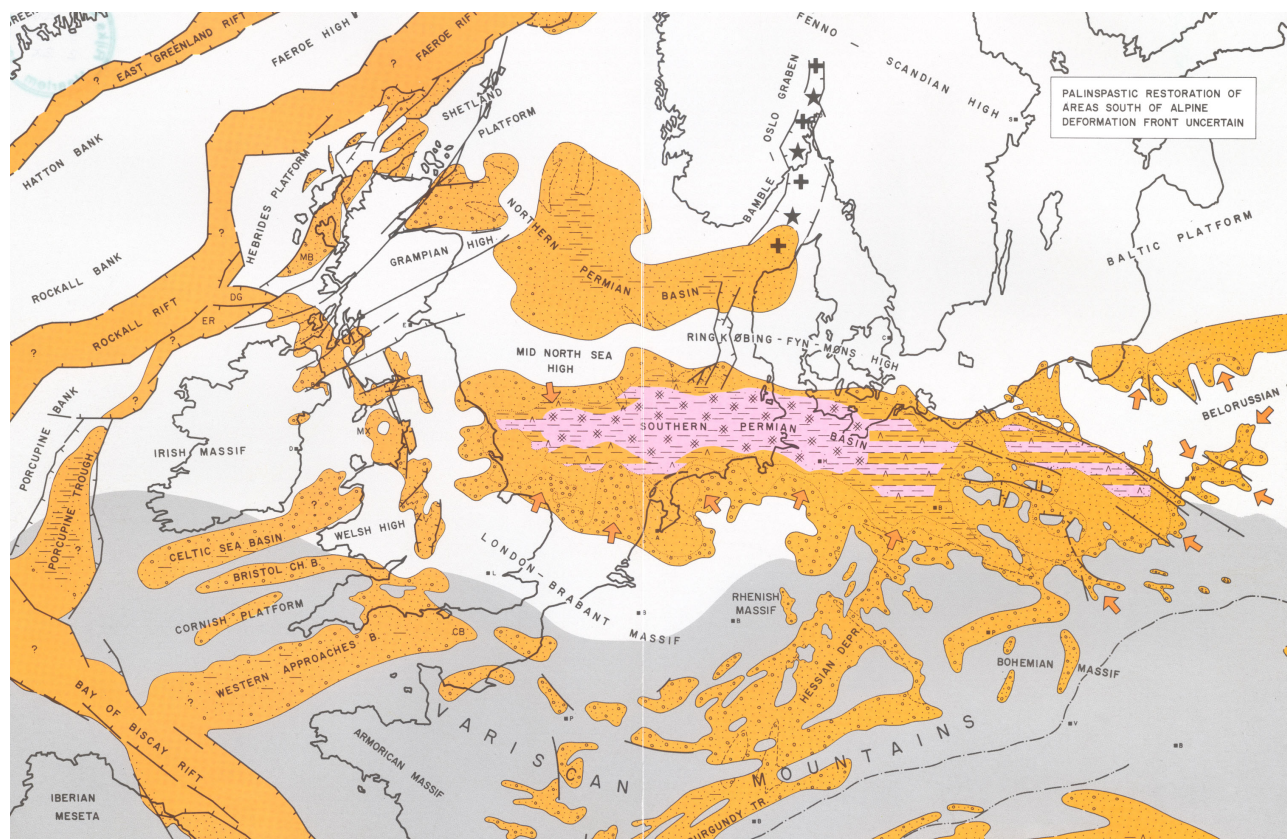


Figure 4: This figure shows the positions of the Northern and Southern Permian Basins during the Early Permian. These basins formed due to thermal subsidence following Carboniferous rifting. Structural highs striking from east to west separate the 2 different basins. For legend see Appendix. Source: Ziegler (1990a)

## 2.4 Late Permian - Triassic

The Late Permian to Early Triassic reactivation of Permian and Paleozoic faults began the onset of the main rifting in the NS. The structural styles of the underlying Paleozoic fault systems indicate reactivation of Variscan and Caledonian thrust sheets [Gibbs (1987), Frost (1987), Cornford and Brooks (1989)]. It is likely that the Mesozoic basins formed due to further reactivation of these Paleozoic rift systems [Lyngsie and Thybo (2007)]. In the Late Permian the Zechstein halites and carbonates were deposited, resulting from periodic inflow from the Arctic Ocean into the southern North Sea and subsequent evaporation [Coward et al. (2003)].

In basinal areas halites were deposited and at basin margins mostly carbonates or anhydrites Ziegler (1990a). Older, rift-related topography controlled the composition and thickness of the Zechstein Group [Jackson and Lewis (2016)]. These varieties in lithological characteristics influenced deformation each subsequent tectonic event had on the formation of the CG [Gowers and Sæbøe (1985), Clark et al. (1998)].

The initiation of rifting in the NS propagating towards the south can be identified by the thickening of Middle



and Late Triassic deposits towards the south. Middle and Late Triassic sequences increase in thickness in the newly forming Dutch Central Graben and Broad Fourteens basin [Ziegler (1990a), Coward et al. (2003)]. The thickening of these sediments can be linked to Zechstein salts withdrawing into structures such as salt pillows and diapirs [van Winden et al. (2018)]. Salt withdrawal affected the depositional patterns of syn-kinematic sediments by forming rim synclines for example [Wong et al. (2007)]. This process is essentially a positive feedback loop. The older, Permian basins striking E-W were overprinted by the N-S basins, transecting the NPB, SPB and MNSH. In the latest Triassic a shift from salt deposits towards clastics is observed in the study area, which may be due to the northward drift of the continents and water supply starting to exceed the rate of evaporation [Hodgson et al. (1992)]. Coarsening upward sequences are observed in the Central Graben in the Late Triassic, indicating a progradation of clastic systems. Sedimentation largely kept pace with the rate of subsidence during the Triassic, thus isopachs give a good estimate of Triassic basin geometries and differential subsidence throughout the basins. These Triassic isopachs shows that the CG was already forming at this point [Ziegler (1982a)].

## 2.5 Early-Middle Jurassic

Following the Triassic extension the southern NS rift system remained active alongside thermal subsidence of the SPB and NPB [Ziegler (1982a), Pharaoh et al. (2010)]. During the Middle Jurassic a thermal dome caused uplift, assumed to result from plume activity on the MNSH triple-rift junction. This formed the Middle North Sea Dome (MNSD) with an area of 700x100km [Underhill and Partington (1993)]. Lower Jurassic and a part of the Triassic sediments were exposed, causing erosion of these lithologies which is known as the Mid-Cimmerian Unconformity [Ziegler (1990b), Underhill and Partington (1993)]. Sedimentation only occurred in the fault-bounded rift basins in this period such as the CG [Husmo et al. (2003), Pieńkowski et al. (2008), Lott et al. (2010)]. Subsequent thermal subsidence during the Middle Jurassic allowed for renewed sedimentation. These sediments mostly consist of coastal-lacustrine and coastal plain deposits up to a few hundred metres thick [Hodgson et al. (1992)]. In the Late Middle Jurassic extension continued in the Bathonian [Coward et al. (2003)].

## 2.6 Late Jurassic - Early Cretaceous

From the Late Jurassic to Early Cretaceous extension accelerated as the stress field changed due to the opening of the Atlantic and the corresponding clockwise rotation of Laurentia-Greenland relative to Eurasia [Torsvik et al. (2002), Ziegler (1988)]. Two different pulses of crustal extension took place in this period. The first rifting pulse lasted from the Bathonian (Middle Jurassic) to the Late Kimmeridgian (latest Jurassic) with a NW-SE direction of extension [Coward et al. (2003)]. The second rifting pulse lasted from the late Kimmeridgian (latest Jurassic) to the Berassian (Early Cretaceous) with a NE-SW extension direction [Coward et al. (2003), Verreussel et al. (2018)]. The change in extensional direction led to NW-SE orientated faults to become reactivated, forming NW-SE transtensional basins [Verreussel et al. (2018), Bouroulllec et al. (2018)].

Observed rim synclines suggest that salt deposits rose towards the surface, piercing younger stratigraphy in the process [Lott et al. (2010), Remmelts (1995)]. The required salt withdrawal in combination with rifting subsidence formed mini-basins [Lott et al. (2010)]. Areas outside the rift basins were uplifted, causing of Triassic and Jurassic deposits on the rift shoulders. The erosional products of these platforms were deposited as fluvio-lacustrine and shallow marine deposits in the CG [Munsterman et al. (2012)].

Rifting ceased in the Early Cretaceous after the second rifting pulse and shifted to the Atlantic domain [Ziegler (1990a)]. After rifting stopped, a period of post-rift sag followed, resulting in subsidence of the CG Ziegler (1990b). Remaining topography was filled during the Early Cretaceous, with post-rift sediments onlapping on the Base Cretaceous Unconformity (BCU), being more mud-prone [Munsterman et al. (2012)]. This further infill of the basin continued up until the Middle Cretaceous, when inversion of the NS began [Rathey and Hayward (1993), Rawson and Riley (1982)]. Subsidence of the basin caused smaller salt structures to subside and feed larger, diapiric structures. The larger salt structures kept downbuilding during the post-rift thermal subsidence, creating condensed section above their heads. This also influenced the depositional facies of later Cenozoic sediments [Hodgson et al. (1992)].

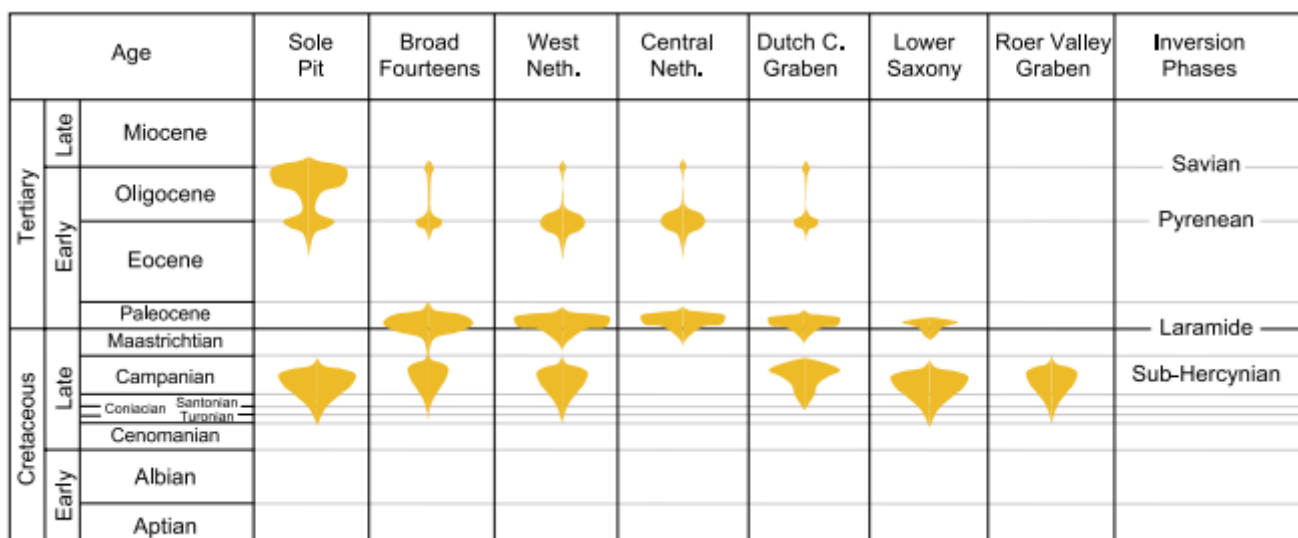


Figure 5: Different inversion phases and their effect on different basins in the Netherlands. For the DCG the Alpine phase during the Late Cretaceous to Paleocene was of main importance. Source: De Jager (2003).

## 2.7 Late Cretaceous - Cenozoic

The Alpine orogeny due to Africa colliding with Eurasia caused northward stress transfer throughout Europe. These contractional stresses caused the inversion of the CG [Rathey and Hayward (1993)]. Pre-existing NW-SE faults were reactivated obliquely due to the general N-S compression resulting from the Alpine inversion [De Jager (2003)]. Apart from the Alpine inversion, the opening of the Atlantic also added to the stress field causing inversion in the CG [Vejbæk and Andersen (2002)]. Different phases of inversion throughout the Cretaceous and Cenozoic influenced the different basins in the Netherlands (Figure 5). While these inversions caused uplift of

the basin centres, the rift shoulders subsided [Littke et al. (2008), Pharaoh et al. (2010)]. The intensity of the inversion decreased towards the north [Heybroek et al. (1975), Dronkers and Mrozek (1991)]. Seismic sections show that Zechstein salts prevented faulting of the supra-salt sequence through strain localization in the salts [Dronkers and Mrozek (1991)]. No clear unconformities are observed from the Early Cenozoic onwards however, which is attributed to thermal subsidence outpacing the inversion [De Jager (2003)]. Throughout the Cenozoic the DCG subsided less than its surroundings, due to which Early Cenozoic deposits are relatively thin [De Jager (2003)].

### 3 Methods

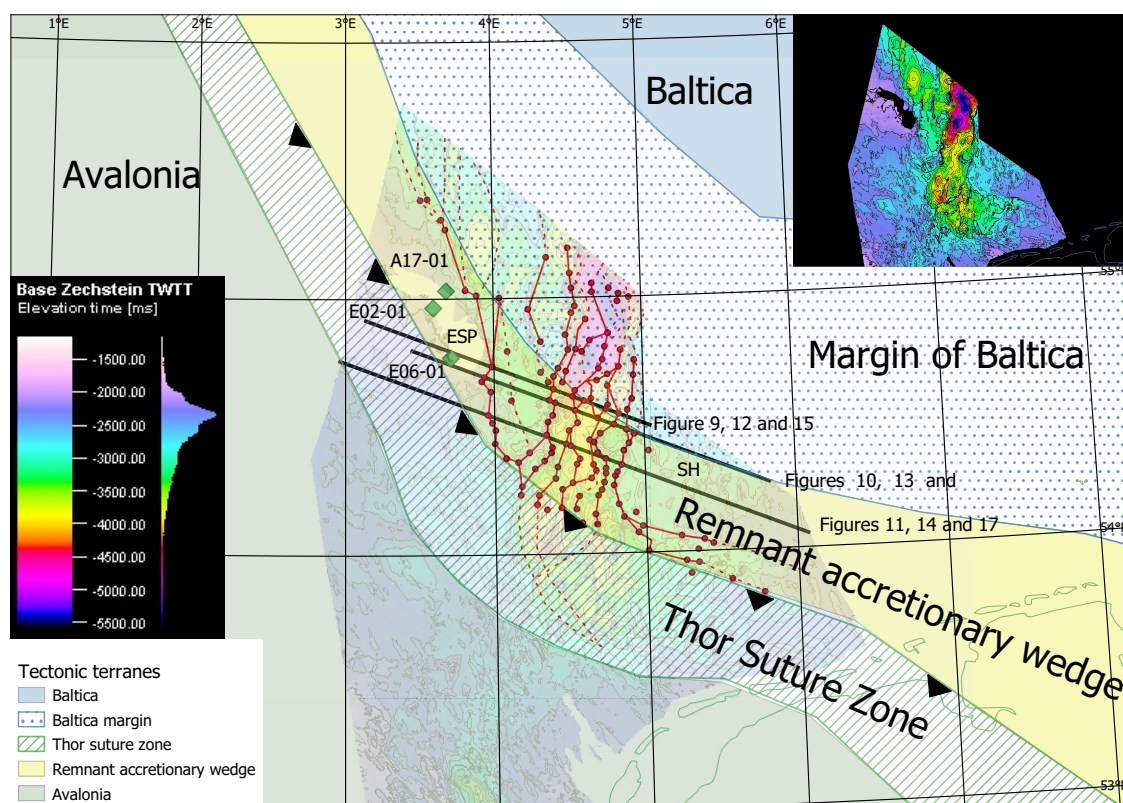


Figure 6: This figure shows an overview of the study area of this research. The underlying colours indicate the depth in TWTT to the base Zechstein which indicates the position of the CG. The area without any base Zechstein date marks the position of the ESP, a structural high in the vicinity of the CG. Overlying the Base Zechstein are the tectonic terranes from Smit et al. (2018). The exact positions of the wells A17-01, E02-01 and E06-01 as well as the seismic lines NSR09-41057, NSR10-11056 and NSR10-41053 used in this research are shown. The red lines are the fault lines within the Paleozoic basement from seismic interpretations made in this study. Dotted parts show extrapolated faults in areas without data and are based on the signature of the base Zechstein surface. The small map in the top right of the map depicts the background image which shows the TWTT to the base of the Zechstein unit. ESP (Elbow Spit High), SH (Schillgrund High)

Interpretations were made of more than 3000km of seismic lines, of which 435km are shown and converted from time to depth to show the corresponding true geometries. Composite lines were made to extend well control of wells A17-01, E02-01 and E06-01 (for exact well locations see Figure 6) where possible, giving a higher level of confidence for the interpretation. For the Paleozoic units seismic facies as defined by ter Borgh et al. (2019)

were used in order to interpret different groups of deposits. The interpretations made were then used to explain the chronological paleotectonic setting in order to explain the formation of the CG and how older structures are related in this development. Qgis 3.4 was used as a tool to make maps showing the overlap of structures in the NS as well as making profiles. Overlaying different maps with different types of data gives insights to structural correlations, allowing for an interpretation with a higher level of confidence.

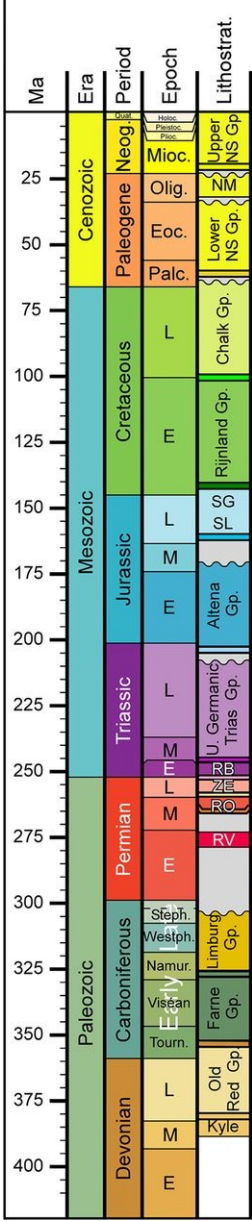


Figure 7: This figure shows the geologic time scale and all the lithostratigraphic units and their respective ages found in the northern Dutch offshore around the area of the Dutch Central Graben and the Step Graben. The same ages for the different lithologies will be used in this research. Source: ter Borgh et al. (2019).

### 3.1 Seismic interpretations

For making seismic interpretations Petrel 2018 is used. Surfaces of the different seismo-stratigraphic units are drawn by following reflective surfaces in the seismic data as well as defining specific seismic facies to a

certain stratigraphic interval. The Paleozoic stratigraphic units (Figure 7) as well as their corresponding seismic facies shown in Figure 8 are used in these interpretations. This is valid because the location of this line is approximately at the same location as the seismic lines shown in Figures 9 and 10. The interpretations of the Mesozoic stratigraphy were largely based on the TNO DGM-deep V3 model, publically available on (<https://www.nlog.nl/dgm-diep-v3-offshore>). Using these constraints an interpretation was made of the subsurface structure in the Dutch offshore in and around the CG. Based on lateral change in seismic facies and a map showing the TWTT of the base Zechstein (DGM-deep V3 offshore, downloadable from <https://www.nlog.nl/en>) were used to define positions of Paleozoic basement faults. For the colour guide of the interpreted seismic units see the Appendix.

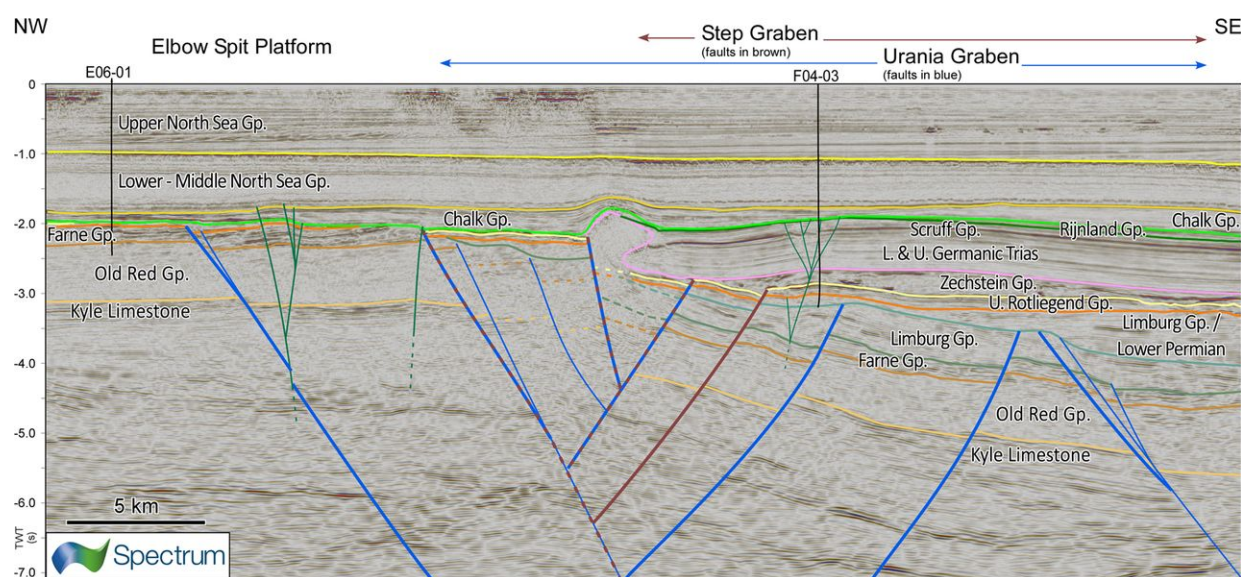


Figure 8: This section shows the seismic facies corresponding to the Mesozoic and Paleozoic stratigraphy defined in Figure 7. The same seismic facies are used in the interpretations along the profiles in this study. Source: ter Borgh et al. (2019).

Most of the interpretations were made on either the NSR10 or NSR09 seismic lines. The NSR09 and NSR10 data set was acquired in the period between 2005 and 2010 as a part of the North Sea Renaissance (NSR) 2D multiclient survey. The lines of both surveys have a spacing of 5.3km and run NE-SW and NW-SE. Acquisition was done with long streamers and a 12.51m spacing between CMPs (exact details on the acquisition can be found on <https://www.nlog.nl/en>). The pre-Zechstein imaging is quite clear, decreasing in quality somewhat where the salt is thicker. Directly underlying large salt diapirs the exact locations of faults or surfaces are hard to determine. In these cases jumps in the base Zechstein are used as an argument for fault placement.

For the lines shown in this research the surfaces of the Base Zechstein as well as the Base Cretaceous chalk are flattened (Section 4.1, Figures 12, 13 and 14). For the sake of simplicity only the most important faults are shown in these figures. The basin configuration at the Permian (Base Zechstein flattened) and the Late Cretaceous (Base Cretaceous chalk flattened) as well as comparing the basin configurations of these different time periods gives insight in the structural development. Horizon flattening will provide some means of justification of the interpretation made. The flattening of a horizon is a simple and fast technique available in most seismic

interpretation software. Disadvantages of horizon flattening include flattening artefacts and distortions [Bland et al. (2004)] as well as not showing the relation of faults with syn-kinematic deposits [Jamaludin et al. (2015)].

### 3.2 Time-depth conversion

For the time to depth conversion VELMOD-3 was used (publically available on <https://www.nlog.nl/en/velmod-31>). VELMOD-3 is composed of seismic velocities acquired through sonic logs and checkshot data which forms a layer-cake velocity model. 3475 velocity data sources were used derived from 1642 different wells. Using equation (1) [Van Dalfsen et al. (2006)], resulting from a linear least squares fit trendline through the  $V_{\text{int-z}_{\text{mid}}}$  method [Robein (2003)], the velocity at depth within each unit is calculated.

$$V = V_0 + kZ \quad (1)$$

In equation (1)  $V$  is the instantaneous velocity in  $[\frac{m}{s}]$  of the lithological unit,  $k$  is the velocity-depth gradient of the lithostratigraphic unit in  $[\frac{m/s}{m}]$  and  $Z$  is the depth where the velocity is calculated in  $[m]$ . Table 1 shows the values for the parameters used for every lithological unit. The parameter  $k$  takes the deformation and decompaction of the lithological intervals into account when calculating their respective velocities. Parameters  $k$  takes into account include (1) initial porosity of the lithology, (2) the decompaction factor, (3) compaction curve following deposition of overlying layers and (4) the bulk rock density [van Winden et al. (2018)]. Table 2 shows the values for the initial porosity, decompaction factor and density for each lithology.

Lithological unit	$K [\frac{1}{s}]$	$V_0 [\frac{m}{s}]$
NU	0.284	1788
NM+NL	0.235	1779
CK	0.593	2646
KN	0.536	2133
SL	0.520	2557
AT	0.436	2259
UGT	0.361	3079
LGT	0.406	3019
LG	0.261	3427

Table 1: This table shows the values of the parameters used in VELMOD-3 to calculate seismic velocities for stratigraphic units. NU (Upper North Sea group), NM+NL (Middle and Lower North Sea groups), CK (Cretaceous Chalk), KN (Rijnland group), SL (Schieland group), AT (Altena group), UGT (Upper Germanic Trias), LGT (Lower Germanic Trias), LG (Limburg group). Source: TNO Velmod-3.1 report, available on <https://www.nlog.nl/en/velmod-31>.

The interval velocity  $V_{\text{int}}$  is the velocity halfway through each lithostratigraphic unit, essentially being the average for the stratigraphic interval. For the Zechstein unit however compaction effects on the  $V_{\text{int}}$  are minor however, due to the Zechstein unit consisting for a large part of anhydrites, halites and carbonates. The Zechstein interval velocity is modelled based on the relation between measured velocity and thickness of the Zechstein unit. Generally for the Zechstein the locations with limited thickness and high carbonate contents show high velocities, while thicker parts with more evaporites generally show a lower seismic velocity as the carbonate

Lithology	Initial porosity	Decompaction factor [ $\frac{1}{km}$ ]	Density [ $\frac{kg}{m^3}$ ]
Sandstone	0.49	0.27	2650
Shale	0.63	0.51	2720
Chalk	0.70	0.71	2200
Salt (halite)	0.00	0.00	2200
Marl	0.50	0.50	2700

Table 2: This table shows the values for initial porosity, decompaction factor and density for each specific lithology found in the North Sea. These parameters are based on data of Verweij et al. (2009) and Fattah et al. (2012).

content decreases. The average velocity values for each of the lithological units were used to calculate the depth to the underlying stratigraphic surface.

Paleozoic velocity-depth trends, apart from the Limburg group, were not calculated in VELMOD-3 due to the sparse data set of the older Paleozoic units. As there is no velocity data available for the deeper seismic facies, velocity values had to be assumed. The velocity of the Early Carboniferous Farne group as well as the velocity of the Late Devonian Old Red group were calculated by adding up constants to the velocity of the Limburg group. This is a valid assumption as generally velocities increase with depth, as the compaction of the lithological units increases. The Kyle limestone was given a constant velocity over the entire basin. The resulting velocities are roughly in agreement with the velocity profile of the MONA LISA 3 profile (Smit et al. (2018)). There is no well data to support the assigned values however. Especially for the Kyle limestone the constant velocity adds the most uncertainty to the solution as the velocity should vary based on the burial depth, which is not applied in the conversion.

After obtaining velocities the following trivial equation is used to calculate the depth of each stratigraphic interval. This function is based on the method following velocity acquisition of the Dix equation (Dix (1955));

$$D_n = D_{n-1} + T_n \quad (2)$$

$$D_n = D_{n-1} + V_n \left( \frac{t_n - t_{n-1}}{2} \right) \quad (3)$$

In this equation  $D_n$  (where  $D_0=0$ , bottom of water column) is the depth of the calculated stratigraphic level,  $V_n$  is the interval velocity of the lithology overlying this stratigraphic interval and  $t_n$  is the travel time of the waves through the lithology. The function does not correct for multiples and assumes a purely vertical ray path. For the depth of the first stratigraphic interval the water depth of the North Sea is added. In order to calculate the true depths the travel time in the lithological unit was halved to correct for the two-way ray path of the waves. This equation was applied at intervals of 25m. Between different points linear interpolation was applied to connect calculated depth points.

Some errors exist in the resulting sections however. In equation (2) uncertainties in the velocity values of the lithological units are incorporated into the final result of the time-depth conversions. As the velocities are more

uncertain increasing with depth, so too decreases the confidence in the resulting converted sections with depth. Faults may be interpreted at the wrong positions in the depth converted sections, as there is an interpolation distance of 25m. Further errors are derived from the seismic interpretation, which serve as the basis for the depth conversion. Another error in the depth conversion is comes from the time surfaces extracted from Petrel. The interpretation software is not able to exactly follow salt structures and cannot incorporate the exact structure. The error in this surfaces is then translated into the depth converted figure.

The depth converted sections are used to check the validity of the interpretation made on the TWTT section, as geometries may or may not make sense when sections are converted from time to absolute depth. The resulting depth sections are used to determine the position and orientation of the large basement faults and to interpret the geometry of the deep structure underlying the CG.

### **3.3 Magnetic and gravity anomalies**

The magnetic and Bouguer anomalies are extracted along the same profiles for which depth conversions are made (publically available on <https://www.nlog.nl/en/gravity-and-magnetic-field>). Values of these anomalies can be related to the presence of volcanics in the subsurface in rifts. Volcanics often contain more ferromagnetic minerals and are less dense than the surrounding medium, causing a positive magnetic anomaly and a negative Bouguer anomaly [Mishra (2011)]. Positive spikes of Bouguer anomalies can be found where high density intrusions are present in the crust [Fowler et al. (1990)]. The observed anomalies can help in constraining locations where volcanics could possibly be present and can be compared to well data. Following Lyngsie and Thybo (2007) the magnetic and gravity data can be used to constrain the deep structure along the profiles.

## **4 Results**

In this study seismic interpretations of tectonic structures in the Paleozoic basement as well as the sub-Zechstein lithostratigraphy on both sides and under the CG are interpreted (Figures 9, 10 and 11, bottom panels). The resulting sections are flattened on the Base Cretaceous Chalk and Base Zechstein surfaces (Figures 12, 13 and 14, middle and bottom panels respectively), as well as being converted to absolute depth to show absolute geometries (Figures 15, 16 and 17).

### **4.1 Seismic interpretations**

#### **4.1.1 Seismic stratigraphy**

The seismic facies below the Kyle limestone [sensu ter Borgh et al. (2019)] on the west side of the sections are separated by erosional surfaces in the seismics lines (Figures 9, 10 and 11, bottom panels). There is no well data on these lithologies however, so the exact age of and the composition of these deposits is unknown. Thus these units will be termed as "Lower Paleozoic". The Lower Paleozoic seismic facies are downthrown towards



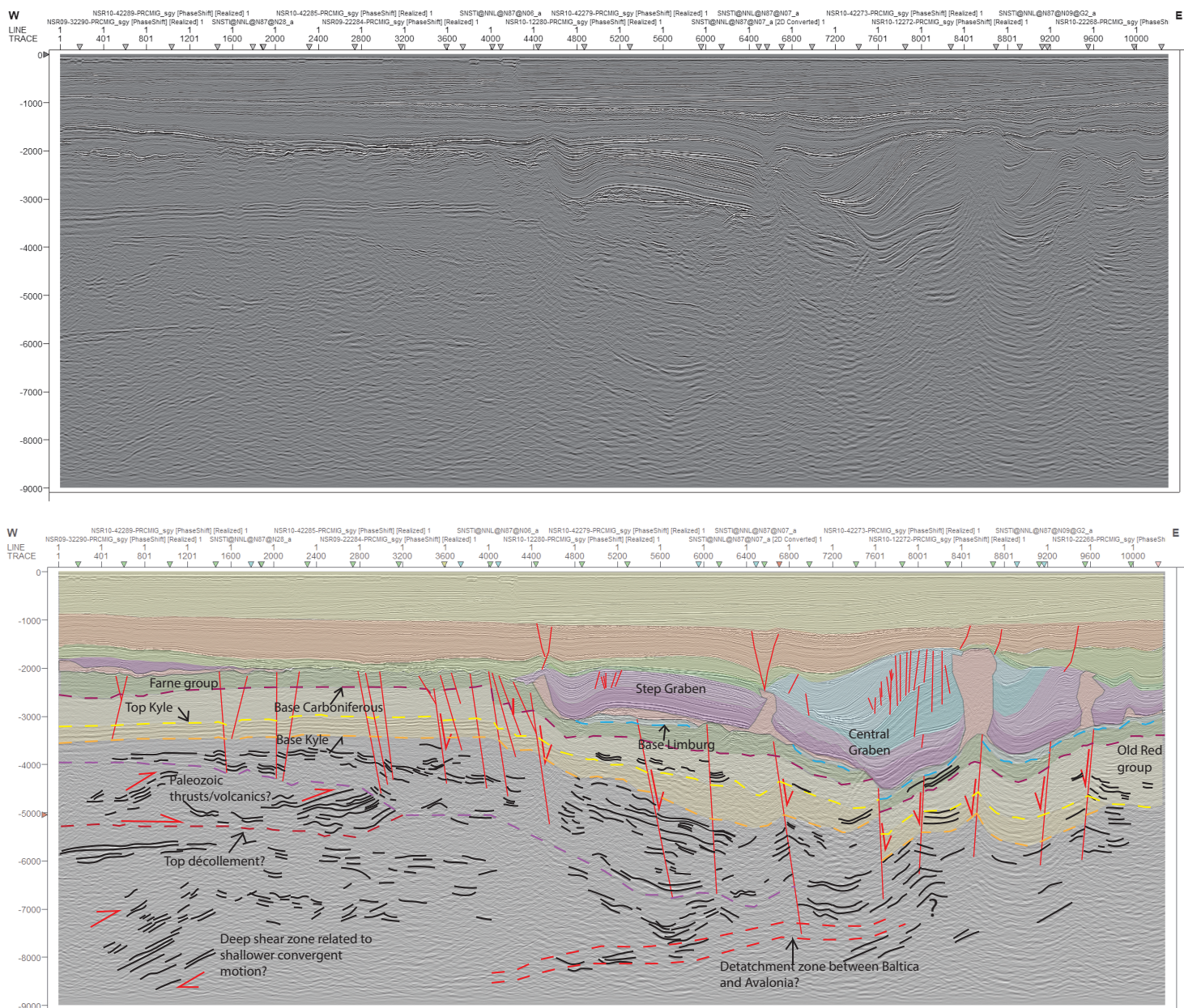


Figure 9: The top panel of the figure shows the uninterpreted version of the seismic line NSR09-41057, the bottom panel shows the interpreted and annotated version of the same seismic line.

the rift system in the east and are cut by the same faults as the Kyle limestone, Old Red group, Farne group and Limburg group units (Figures 9, 10 and 11). On the western side of the sections wedge shaped bodies can be distinguished on the northern lines (Figures 9 and 10, bottom panels), underlain by a strong and relatively continuous reflector. The reflectors in this wedge are somewhat chaotic and have a relative shallow dip to the west on the western side of what seems to be a crest and a more steep dip to the east on the eastern side of this crest (Figures 9 and 10, bottom panels). These reflectors are really bright, as their amplitudes are way higher than those of the surrounding material which shows a more homogeneous seismic facies. This wedge shape is not observed on the seismic line in the more southern part of the CG however, where instead at the same depth different sets of reflectors terminate unconformably with an onlapping structure (Figure 11). The seismic facies

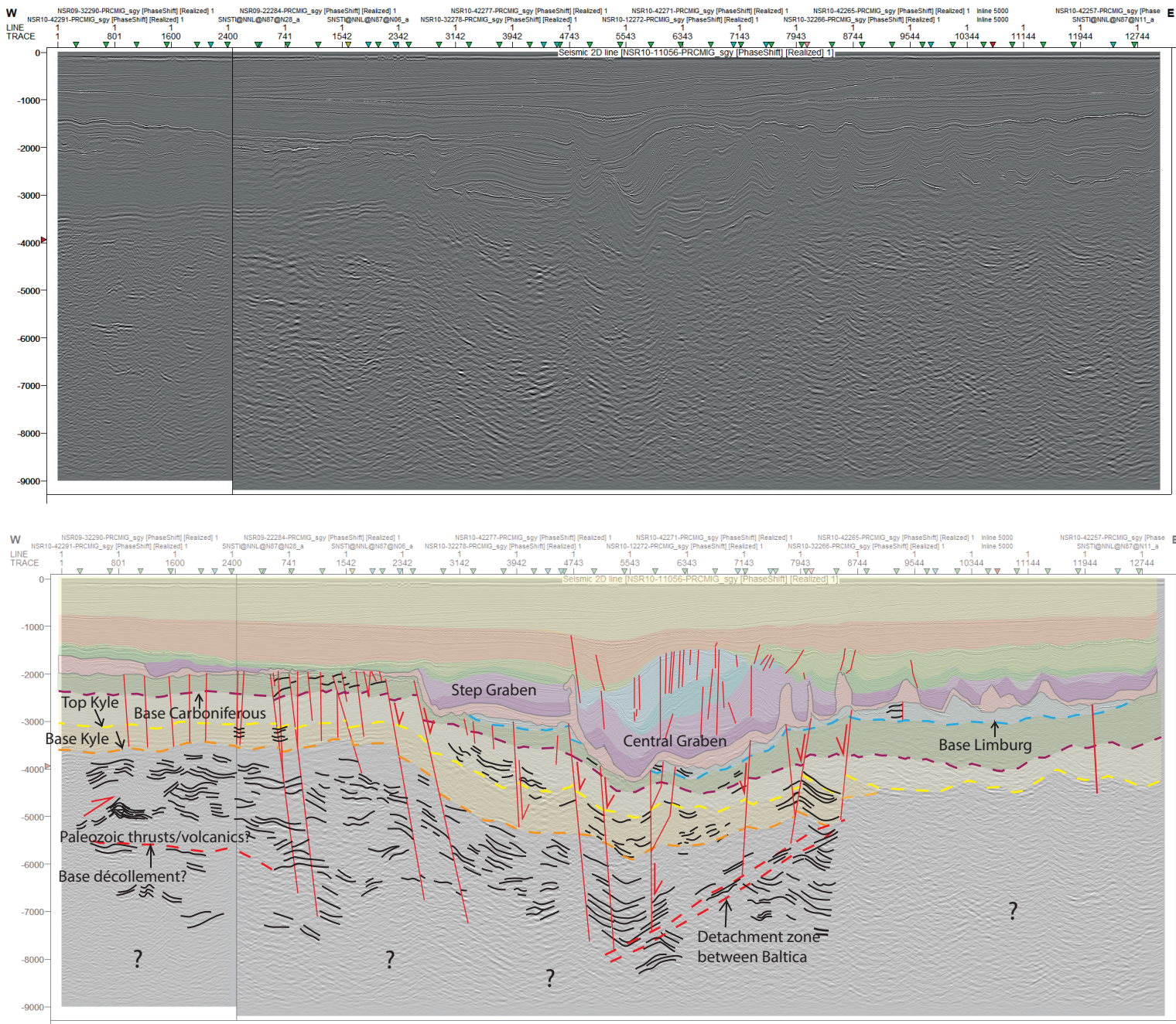


Figure 10: The top panel of this figure shows the uninterpreted version of the seismic lines NSR10-11056, the bottom panel shows the interpreted and annotated version of the same seismic line.

underlying the Kyle limestone and Old Red group east of the CG do not show any structures nor layering which is as clear west of the SG at the same depth and is generally more chaotic and homogeneous (Figures 9, 10 and 11, bottom panels).

West of the SG the Kyle limestone, Old Red group, Farne group and Limburg group [sensu ter Borgh et al. (2019)] are observed which are separated by erosional surfaces (Figures 9, 10 and 11, bottom panels). Thicknesses for the Kyle limestone, Old Red group and Farne group are uniform, except where these units are offset by normal faults where thickness increases on the downthrown side of the fault (Figures 9, 10 and 11, bottom panels). From the western margin of the SG the Kyle limestone thickens towards the CG for the northern lines (Figures 9 and 10, bottom panels) but thins somewhat towards the CG for the southern line (Figures 11, bottom

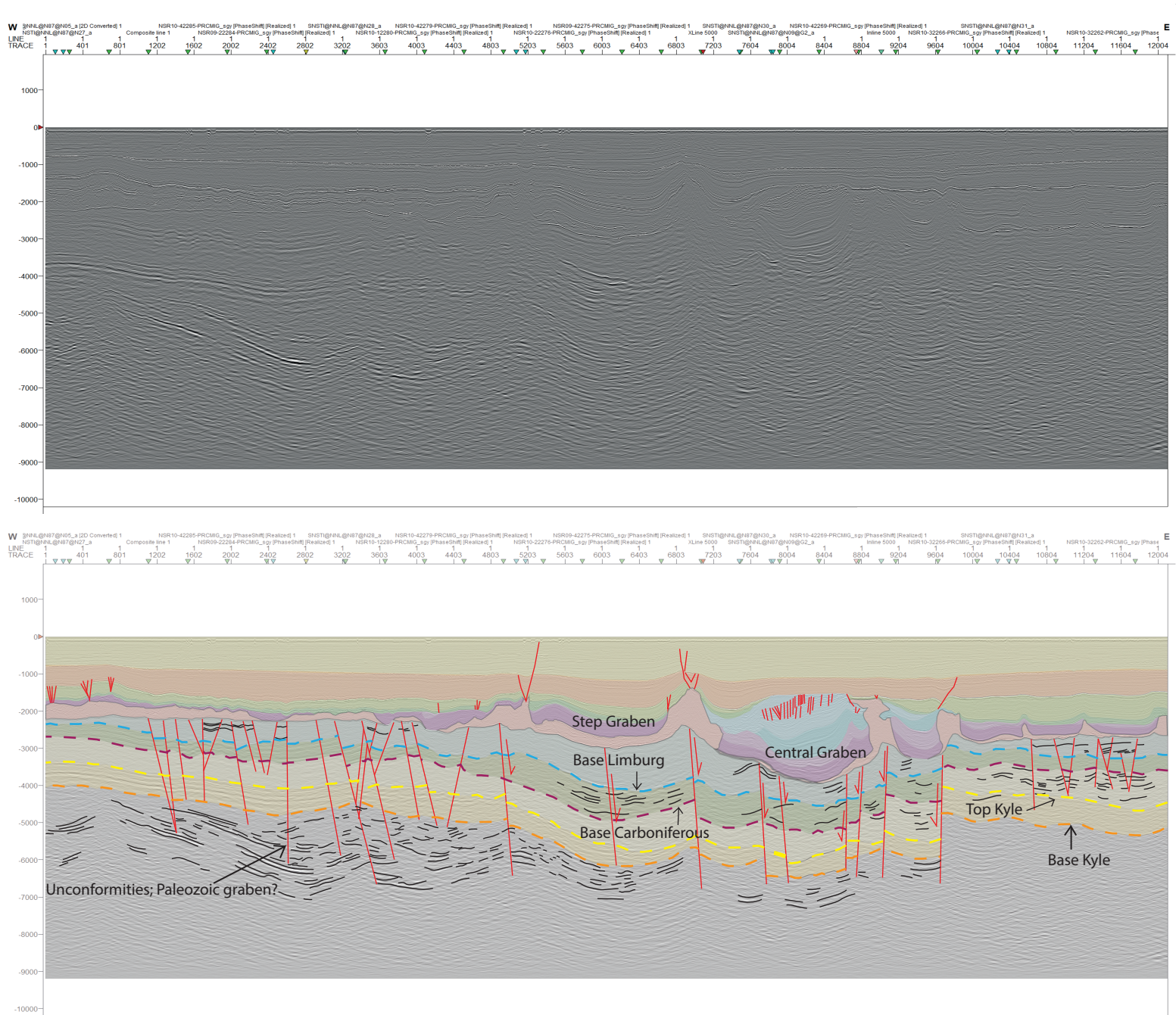


Figure 11: The top panel of this figure shows the uninterpreted version of the seismic line NSR10-41053, the bottom panel shows the interpreted and annotated version of the same seismic line.

panel). Only small areas of the Limburg group are observed in the northern lines under the SG and CG (Figures 9 and 10, bottom panels). In the southern line the Limburg group is observed along the entire profile (Figure 11, bottom panel). The Farne group and Kyle limestone seismic facies show high amplitude low frequency layering on the west side of the sections, while the Old Red group is more homogeneous at the lower side and shows some low amplitude layering towards the top (Figures 9, 10 and 11, bottom panels). The Limburg group show more homogeneous seismic facies with low amplitude layering over the entire seismic facies (Figures 9, 10 and 11, bottom panels).

Under the SG the layered seismic facies of the Kyle limestone and Farne group is still preserved, although the clear layered structure is less evident as the seismic facies becomes progressively more chaotic towards the east (Figures 9, 10 and 11, bottom panels). Under the CG, where the Kyle limestone, Old Red group, Farne

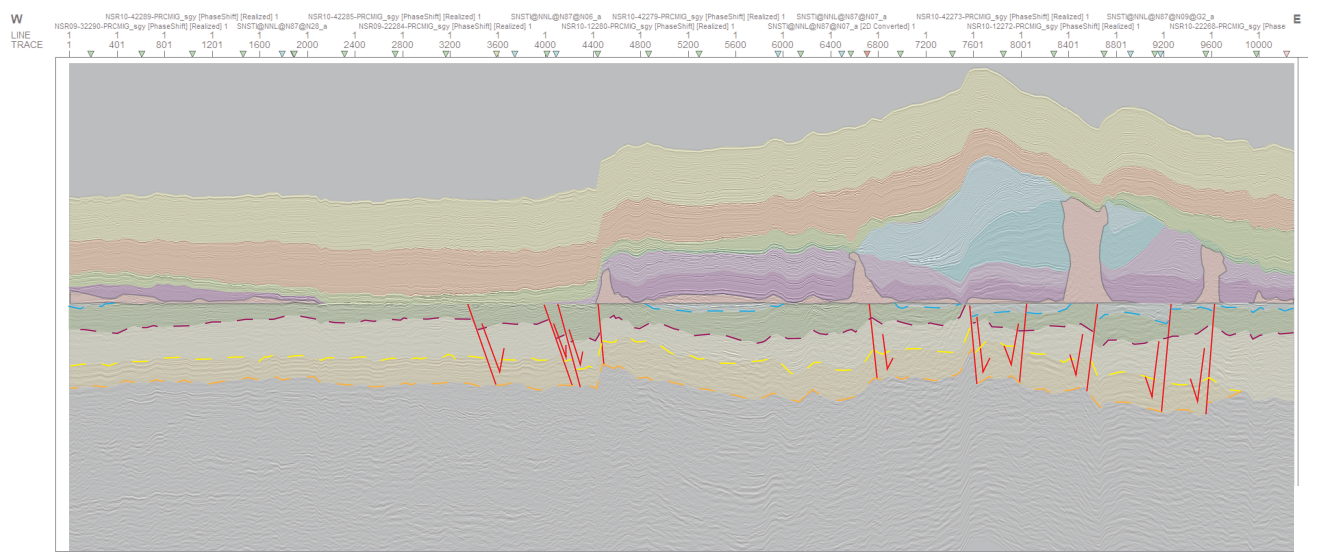
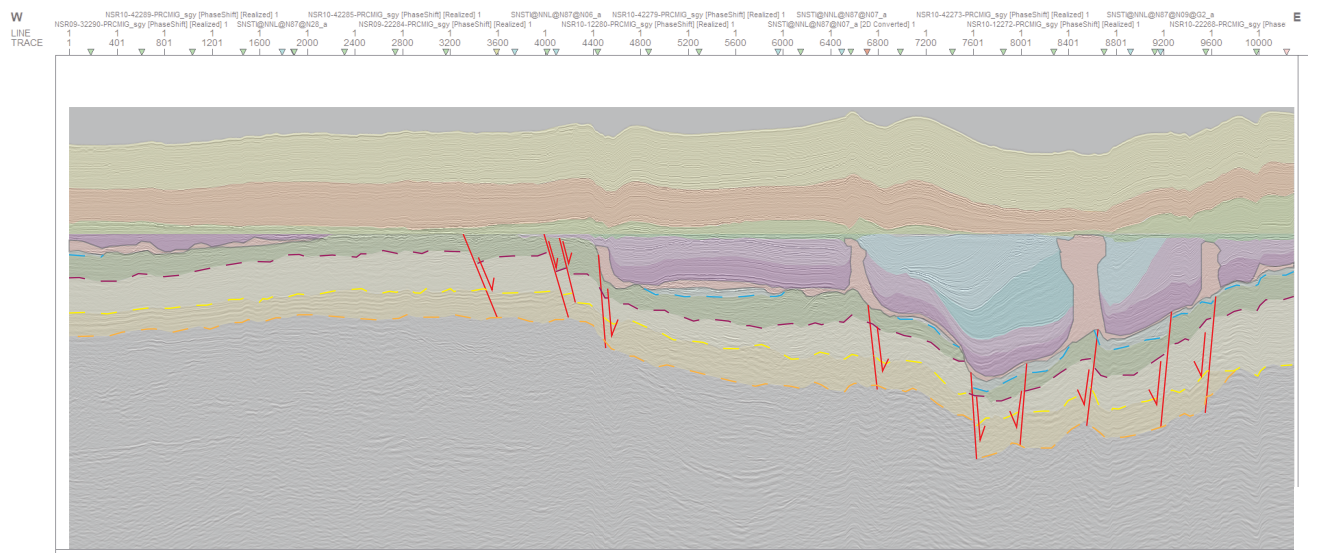
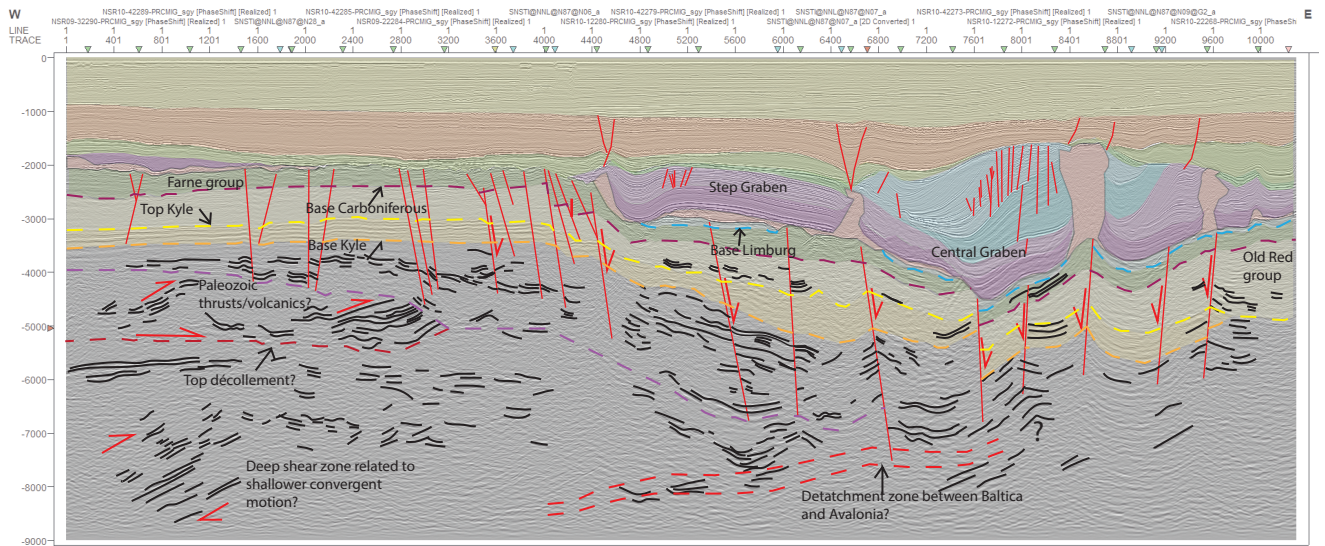


Figure 12: The top panel of this figure shows the interpreted line drawing of NSR09-41057. The middle panel shows the same seismic section when flattened on the Base Cretaceous chalk surfaces and the bottom panel shows the section when flattened on the Base Zechstein surface.

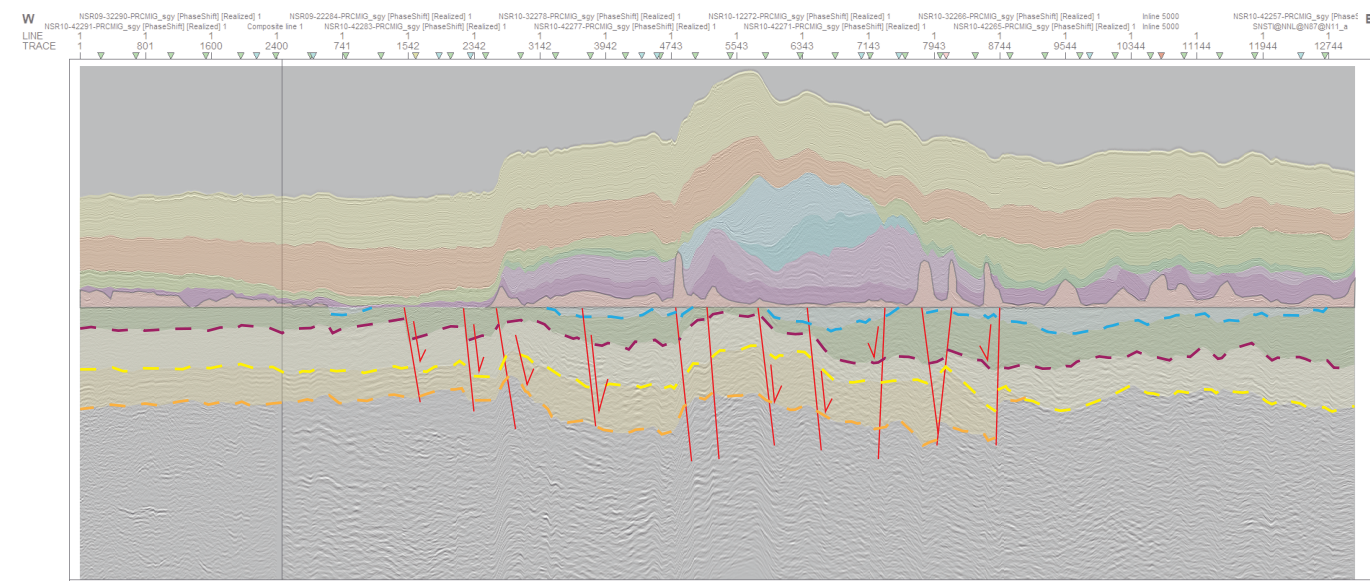
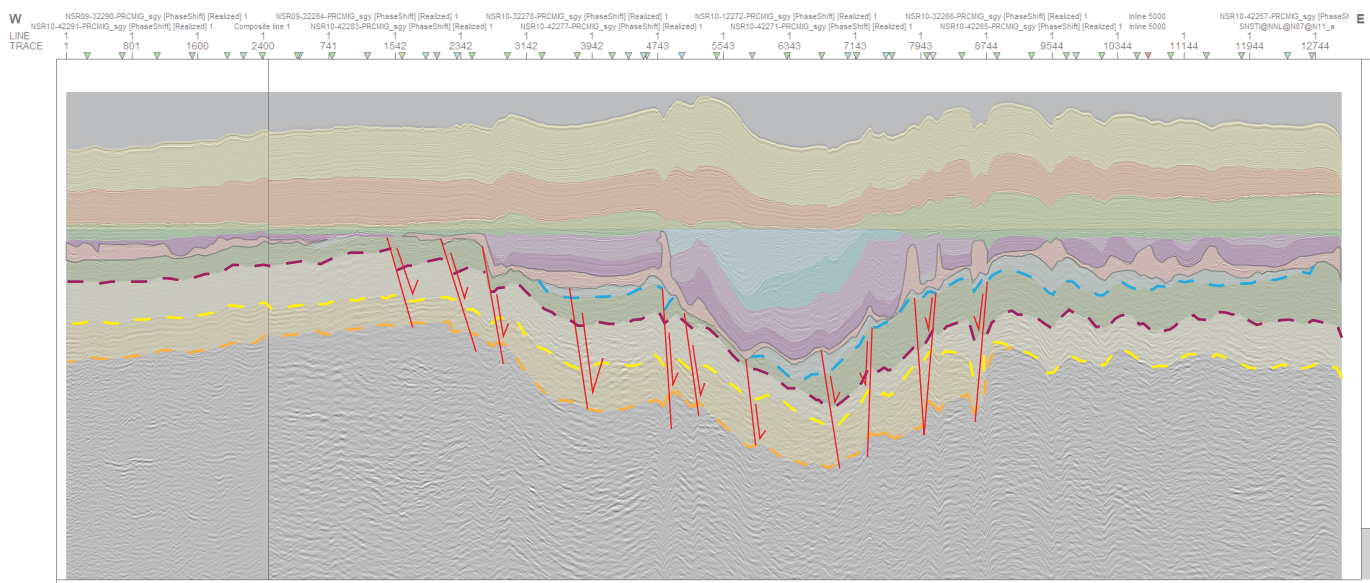
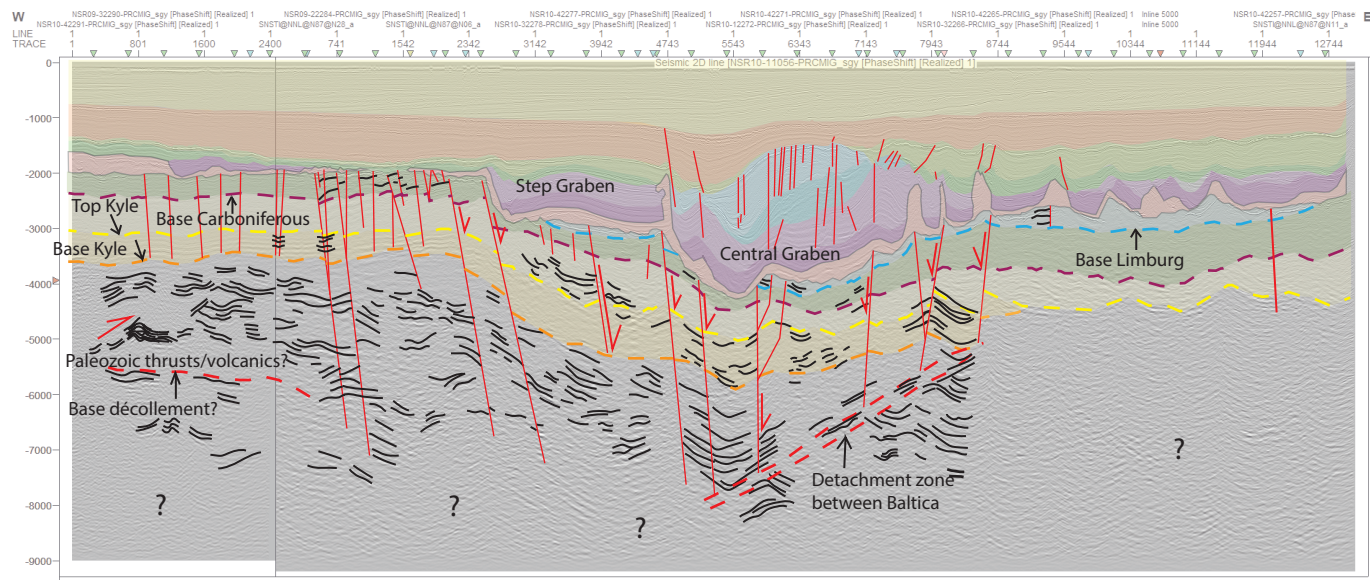


Figure 13: The top panel of this figure shows the interpreted line drawing of NSR10-11056. The middle panel shows the same seismic section when flattened on the Base Cretaceous chalk surfaces and the bottom panel shows the section when flattened on the Base Zechstein surface.

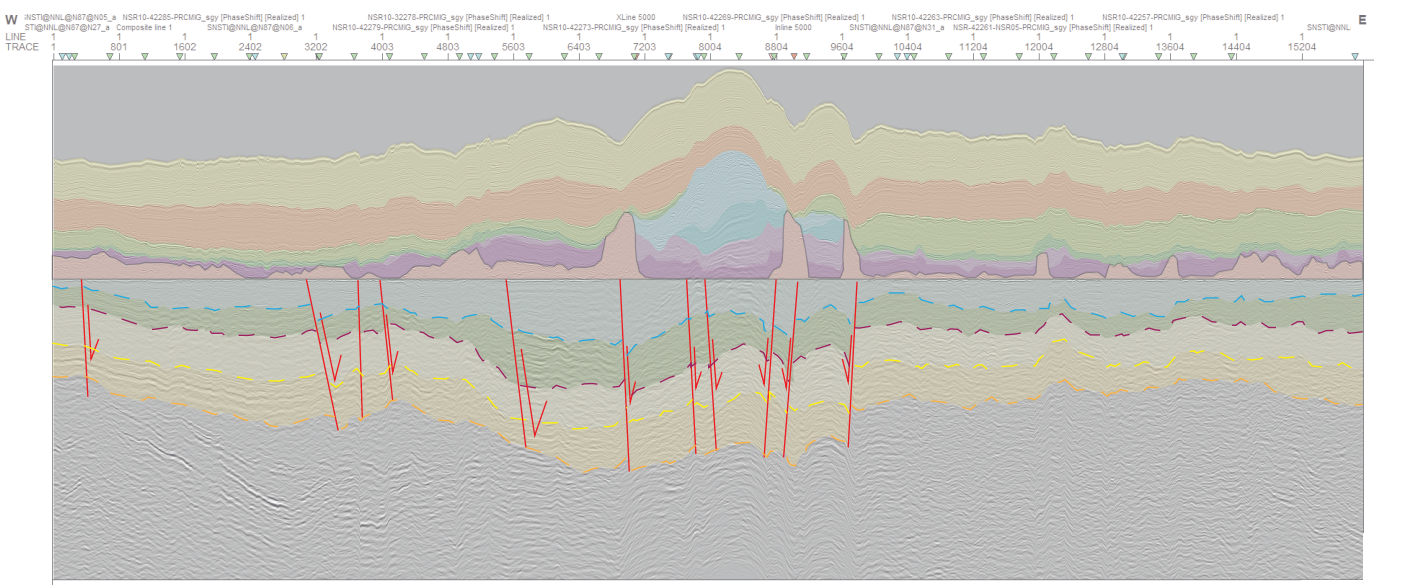
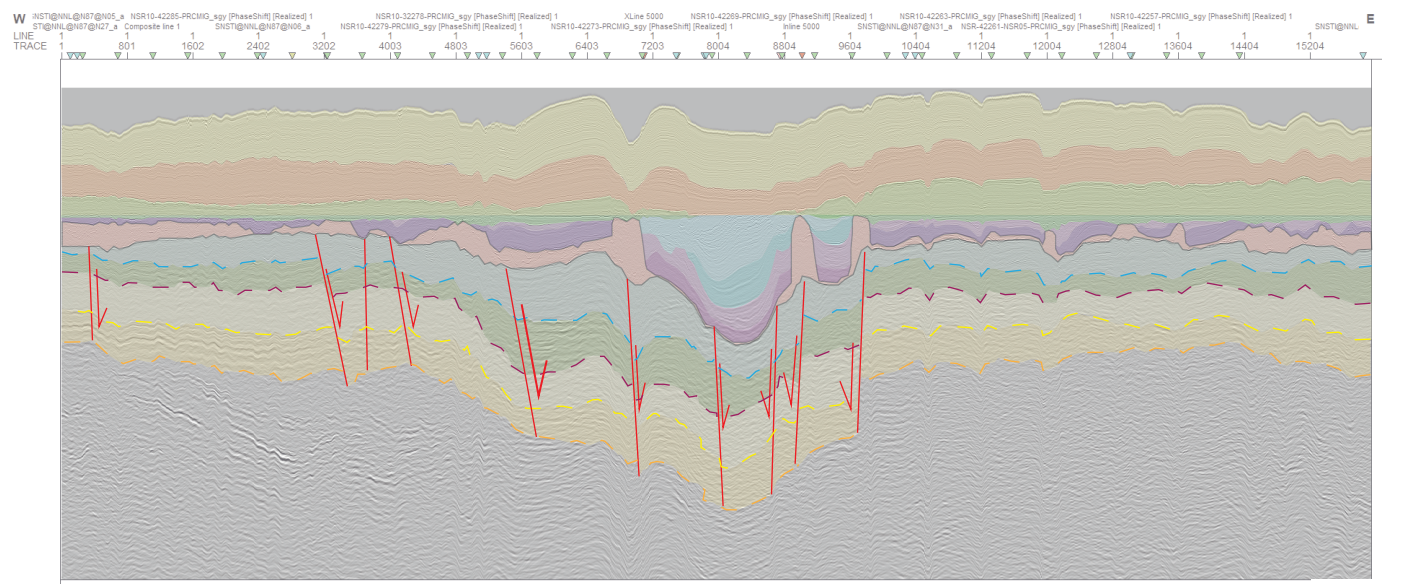
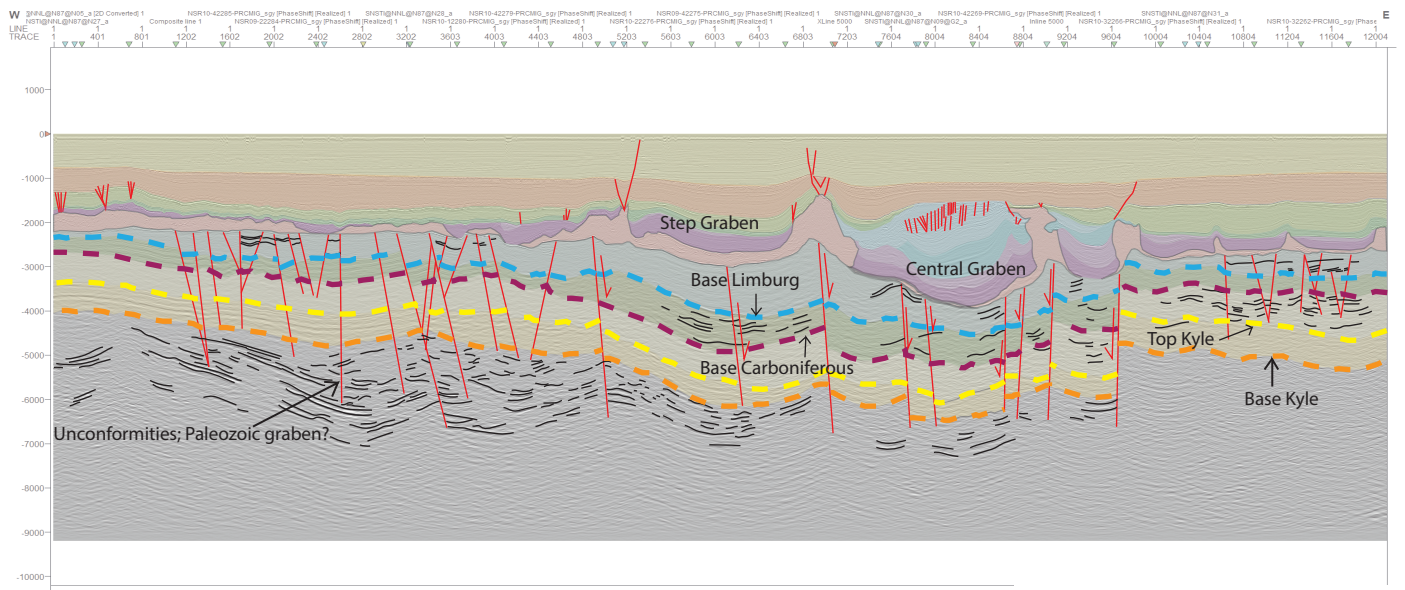


Figure 14: The top panel of this figure shows the interpreted line drawing of NSR10-41053. The middle panel shows the same seismic section when flattened on the Base Cretaceous chalk surfaces and the bottom panel shows the section when flattened on the Base Zechstein surface.

group and Limburg group are at the greatest depths, the seismic facies are mainly chaotic (Figures 9, 10 and 11, bottom panels). Some small areas showing characteristic layering facies for the Kyle limestone and Farne group indicate that there is a lateral continuity between the western side of the section and the deposits under the CG (Figures 9, 10 and 11, bottom panels). The Old Red group, Farne group and Limburg group can be correlated from the western side of the CG to the eastern side of the CG (Figures 9, 10 and 11, bottom panels). The Kyle limestone can't be correlated from west to east under the CG for the northern sections (Figures 9 and 10, bottom panels) but it is possible for the southern section (Figure 11, bottom panel). The seismic facies for some of these units differs east of the CG from what is observed west of the CG. The Old Red group generally shows more internal reflectors on the east side (Figures 9, 10 and 11, bottom panels). The Kyle limestone, where present east of the CG, and the Farne group don't show the clear layered structure observed west of the CG (Figures 9 and 10, bottom panels). The seismic facies of the Limburg group does not show changes in seismic facies when comparing the different sides of the CG however (Figure 11, bottom panel). The observed changes in seismic facies for the Kyle limestone, Old Red group and Farne group comparing west to east are less evident for the southern line (Figure 11, bottom panel).

The Old Red group and Farne group show varying thickness changes from the west side of the SG to the eastern side of the CG, thickening across some faults while thinning across others (Figures 9, 10 and 11, bottom panels). For the northern lines these units increase in thickness under the SG followed by thinning further towards the CG (Figures 9 and 10, bottom panels). For the southern line the Old Red group shows some thickening from the western margin of the SG towards the eastern margin of the CG while the increase in thickness from the Farne group along the same part of the profile is more significant (Figure 11, bottom panel). The Limburg group thickens the most towards the east of all the units followed by thinning from the western margin of the CG to the eastern limit of the section (Figure 11, bottom panel). Generally the combined thickness is larger under the SG and CG than on the eastern or western sides of the rift system (Figures 9, 10 and 11, bottom panels). East of the CG thickness changes are observed for the Kyle limestone, Old Red group, Farne group and Limburg group, but they are cut by only a few faults compared to the amount of faults west of the SG (Figures 9 and 11, bottom panels).

The Mesozoic stratigraphy overlies the Zechstein unit and lateral differences in thickness along the seismic sections for most of the depositional sequences are observed (Figures 9, 10 and 11). Jumps in the Mesozoic stratigraphy in the SG and CG are consistent with the location of underlying basement faults and are folded and tilted rather than faulted (Figures 9, 10 and 11, bottom panels). Lower Triassic sediments do not show any thickness changes nor any faults in the CG (Figures 9, 10 and 11). West of the SG and east of the CG the Lower Triassic deposits are found in local depocenters bound by salt structures (Figures 9, 10 and 11). In contrast to the Lower Triassic deposits, the Upper Triassic deposits do show faulting and thickness changes in the CG (Figures 9, 10 and 11).

The thickness of the Jurassic sediments is larger than the thickness of the Triassic deposits (Figures 9, 10 and

11, bottom panels). Both the Altena and Schieland groups thicken from the west side towards the central and eastern parts of the CG (Figures 9, 10 and 11, bottom panels). The Jurassic deposits in the CG show normal faults with offsets in the order of 10 to 20ms (Figures 9, 10 and 11, bottom panels). Jurassic deposits are not found in the SG, west of the SG or east of the CG, as Triassic deposits are directly overlain by Cretaceous deposits (Figures 9, 10 and 11, bottom panels). Cretaceous deposits are observed along the entire length of the profiles except where they pinch out against the pop-up structure in the CG (Figures 9, 10 and 11, bottom panels).

Outside of the CG and SG the thickness of the Mesozoic sequence differs the western and eastern sides of the seismic lines (Figures 9, 10 and 11, bottom panels). The east side shows a larger Mesozoic thickness than the west side, with the Cretaceous chalk having the largest thickness (Figures 9, 10 and 11, bottom panels). The Cretaceous deposits unconformably overlie the Triassic deposits on both sides of the rift system (Figure 9, 10 and 11, bottom panels). Faulting of the Mesozoic sequence outside the rift system is only observed directly above salt structures (Figures 9,10 and 11, bottom panels).

The Lower, Middle and Upper North Sea groups are generalized into a single unit. These sequences only show thickness changes above salt structures and the pop-up structure in the CG and have a constant thickness on the rift shoulders (Figures 9, 10 and 11, bottom panels). Faulting is only observed directly above salt structures (Figures 9, 10 and 11, bottom panels).

#### **4.1.2 Faults and structures**

An unconformity under the CG is observed for the Lower Paleozoic units where truncations against a surface can be observed, marked by a red dashed line (Figures 9 and 10, bottom panels). The basement faults do not cut through this unconformity (Figures 9 and 10, bottom panels). The geometry of this surface is not the same for the different seismic lines where it is observed, with ramps and flats alternating in the northernmost lines where reflectors above the unconformity bend upward and underlying reflectors follow the trend of the unconformity (Figure 9, bottom panel). For the other section a relatively steep and continuous surface is observed where reflectors above the unconformity bend upward and the reflectors below the unconformity bend upward and truncate against the unconformity (Figure 10, bottom panel). This unconformity is not observed in the southern section (Figure 11, bottom panel).

West of the SG downthrown blocks are observed where the Kyle limestone, Old Red group, Farne group and Limburg group are offset by faults with hanging walls towards the east (Figures 9, 10 and 11, bottom panels). Across the faults of the downthrown blocks the Farne group and Limburg group show an increase in thickness (9 and 11, bottom panels). The same units are cut by fewer faults east of the CG and do not show the same downthrown block structures (Figures 9 and 10, bottom panels). Under the CG large basement faults cut the Kyle limestone, Old Red group, Farne group and Limburg group (Figures 9, 10 and 11, bottom panels). These basement fault strike N-S (Figure 6). West of the graben axis of the CG these faults dip towards the east and



vice versa (Figures 9, 10 and 11, bottom panels). The largest offset is observed at the easternmost fault under the CG (Figures 9, 10 and 11, bottom panels). The northernmost line also shows a relatively large offset at the center of the CG at trace 7601 (9, bottom panel). The basement faults do not cut through the Permian Zechstein unit and show offsets for the Paleozoic in the order of a couple 100ms (Figures 9, 10 and 11, bottom panels). Large salt structures are observed above the fault tips (Figures 9, 10 and 11).

When flattening on the base Zechstein unit the Paleozoic shows a half-graben structure below the future locations of the CG and SG (12, 13 and 14, bottom panels). The thickness of the Paleozoic units increases from western margin of the SG to the easternmost fault bounding the CG on some seismic sections (Figures 12 and 14, bottom panels). West of the SG the Kyle limestone, Old Red group, Farne group and Limburg group shallow somewhat of which Figure 10 (bottom panel) shows the best example (Figures 9, 10 and 11, bottom panels). When the downthrown blocks west of the rift system are observed it is observed the the Kyle limestone does not any thickness changes across these faults, while the Old Red group, Farne group and Limburg group show thickness changes across the normal faults (Figures 12, 13 and 14, bottom panels). The offsets are generally largest for the Farne group and Limburg group (Figures 12, 13 and 14, bottom panels).

The Paleozoic stratigraphy was not downthrown as much at the location of the SG compared to the CG (Figures 12, 13 and 14, middle panels). On the western side of the sections the Paleozoic shallows towards the east until reaching the western margin of the SG (Figures 12, 13 and 14, middle panels). The thickness of the Mesozoic and Paleozoic stratigraphy combined thickens from the west side of the sections until the eastern margin of the CG with a half-graben structure, with the maximum thickness being in the center of the CG (Figures 12, 13 and 14, middle panels). When comparing the middle panels to the bottom panels of Figures 12, 13 and 14 the rift system is more asymmetric in the Mesozoic. What is striking are the decreasing thicknesses of the Cretaceous Chalk and Lower- and Middle NS groups directly above the CG. Thicknesses of the Cretaceous Chalk and the entire NS supergroup also decrease directly above diapirs (Figures 12, 13 and 14, middle panels).

## 4.2 Time-Depth conversion combined with gravity and magnetic anomalies

Figures 15, 16 and 17 show the time to depth converted seismic sections of lines shown in Figures 9, 10 and 11 respectively in the top panels and the proposed crustal structures in the bottom panels. The thick green line represents the depth to the moho and is observed to shallow eastward (Figures 15, 16 and 17, top and middle panels). The proposed crustal structures are based on the profile shown by [Lyngsle and Thybo (2007)] and the terranes defined by Smit et al. (2016), as well as gravity and magnetic anomaly data along these profiles (Figures 15, 16 and 17, bottom panels) and seismic interpretations. Thickening from the western margin of the section to the eastern margin of the CG is observed for the Paleozoic (Figure 15, top panel) and Mesozoic (Figures 15, 16 and 17, top panels).

The Bouguer anomalies on the western side of all 3 sections show decreasing values further towards the west and show low values compared to the SG and CG areas (Figures 15, 16 and 17, bottom panels). The Bouguer

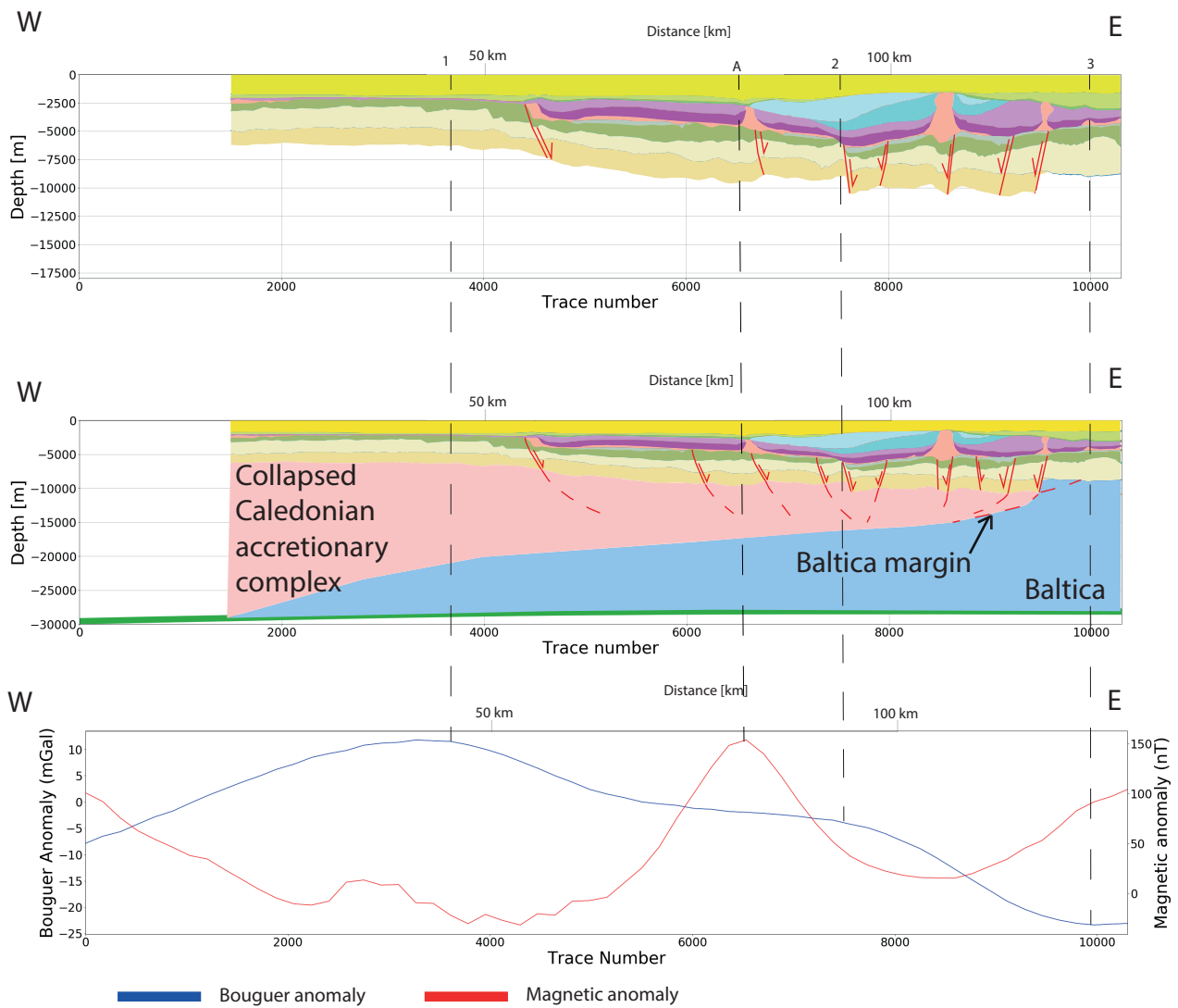


Figure 15: This figure shows the result of the time to depth conversion of the seismic line NSR09-41057. The same color code is applied as in the line drawings. The top panel of this figure shows the result of the time to depth conversion for the line drawing of NSR09-41057 without any further interpretation. The middle panel shows the interpretation at crustal scale and shows the deep continuation of the major normal faults as dotted lines as well as the underlying terranes. Deep profile interpretation based on [Lyngsle and Thybo (2007)], anomaly data and seismic facies. The thick green line at the bottom represents the Moho. The bottom panel shows the magnetic and gravity anomalies along the same profile. Solid lines annotated with numbers give parts along the profile where such gradients are observed, dashed lines annotated with letters give the locations of spikes in the magnetic anomaly.

anomaly is negative in the line in the southern part of the CG (Figure 17, bottom panel) as opposed to the sections further north showing positive values at the SG and CG (Figures 15 and 16, bottom panel). All Bouguer anomaly graphs follow the same trend however, being relatively constant (0 to -5mGal) underneath the CG and showing a stepwise decrease towards the east. Line 1 and 2 in Figure 15 correspond to the area where the seismic facies of the Paleozoic units transition laterally to a more chaotic facies (Figure 9, bottom panel). Crossing line 2 the CG deepens significantly (Figure 15, top panel) and crosses the boundary of 2 different tectonic terranes (Figure 6). For Figure 16 line 1 and 2 mark the margins of the CG and when crossing line 2 the corresponding seismic section overlies the boundary between different tectonic terranes (Figure 6). For Figure 17 line 1 and 2

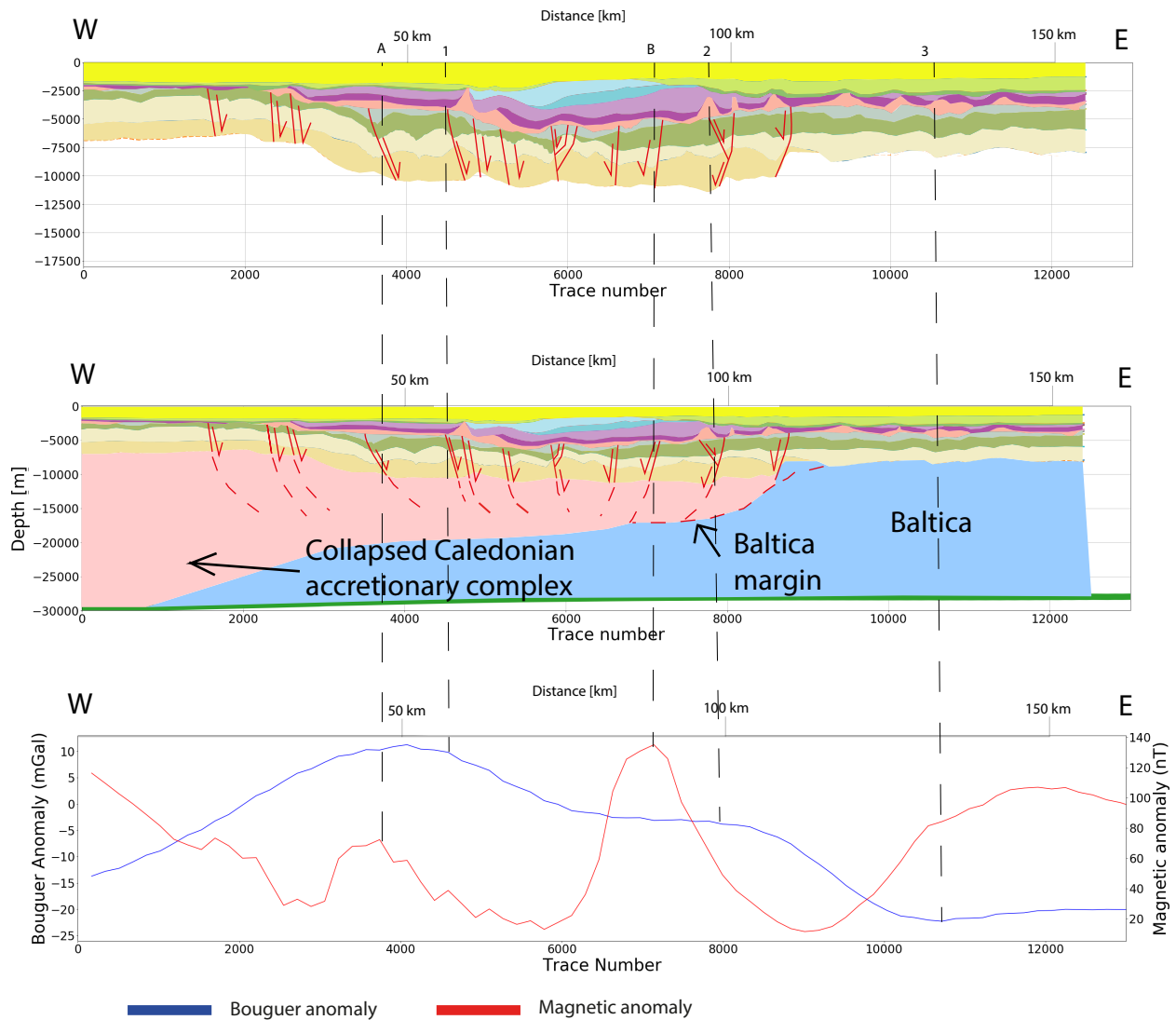


Figure 16: This figure shows the result of the time to depth conversion of the seismic line NSR10-11056. The same color code is applied as in the line drawings. The top panel of this figure shows the result of the time to depth conversion for the line drawing of NSR10-11056 without any further interpretation. The middle panel shows the interpretation at crustal scale and shows the deep continuation of the major normal faults as dotted lines as well as the underlying terranes. Deep profile interpretation based on [Lyngsle and Thybo (2007)], anomaly data and seismic facies. The thick green line at the bottom represents the Moho. The bottom panel shows the magnetic and gravity anomalies along the same profile. Solid lines annotated with numbers give parts along the profile where such gradients are observed, dashed lines annotated with letters give the locations of spikes in the magnetic anomaly.

mark the margins of the rift system and from line 2 to 3 overlies the Schillgrund High.

All observed magnetic anomalies are positive, apart for a small segment along the northernmost section (Figures 15, 16 and 17). Generally the magnetic anomaly shows relatively high positive values towards the western margins of the profiles, decreasing in value towards the rift system to the east (Figures 15, 16 and 17). The low values in the rift systems are perturbed by local positive spikes at the western margin of the CG (Figure 15), at the SG and central part of the CG (Figure 16) and western rift shoulder (Figure 17). The eastern rift shoulder generally shows continuous positive values in the order of 100 nT for the northern sections (Figures 15 and 16, bottom panel) and positive spikes in the order of 100 nT with lower positive values between spikes

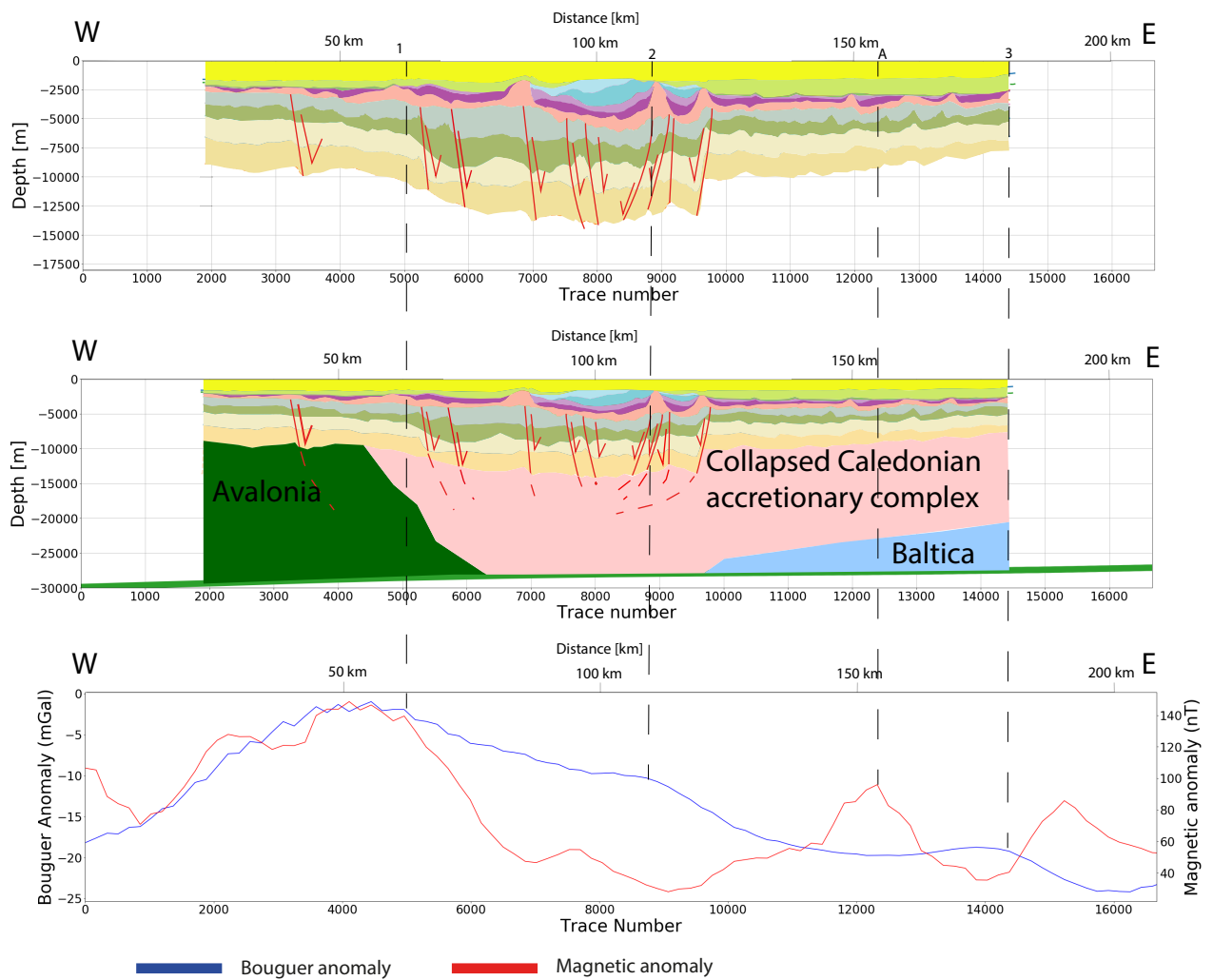


Figure 17: This figure shows the result of the time to depth conversion of the seismic line NSR10-41053. The same color code is applied as in the line drawings. The top panel of this figure shows figure shows the result of the time to depth conversion for the line drawing of NSR10-41053 without any further interpretation. The middle panel shows the interpretation at crustal scale and shows the deep continuation of the major normal faults as dotted lined as well as the underlying terranes. Deep profile interpretation based on [Lyngsle and Thybo (2007)], anomaly data and seismic facies. The thick green line at the bottom represents the Moho. The bottom panel shows the magnetic and gravity anomalies along the same profile. Solid lines annotated with numbers give parts along the profile where such gradients are observed, dashed lines annotated with letters give the locations of spikes in the magnetic anomaly.

(Figure 17). The magnetic spikes A for in Figure 16 corresponds to some bright reflectors observed in the Old Red group under the SG (Figure 10, bottom panel). Line A and line B in Figures 15 and 16 respectively do not show any bright reflectors, but are located in the vicinity of faults. The position of line A in Figure 17 is not shown on the line drawing of the corresponding section.

## 5 Discussion

### 5.1 Crustal structure of the CG

The seismic facies below the Kyle limestone for the northern lines (Figures 9 and 10, bottom panels) are suggestive for volcanic material. They are inclined and have high amplitudes compared to the surrounding material. The negative Bouguer anomalies (-10 to -15mGal) and positive magnetic anomalies (100 to 120nT) at the corresponding traces (Figures 15 and 16, bottom panels) support this interpretation. These volcanics may be equivalents of the Famennian volcanics found on the northern flank of the ESP [Lundmark et al. (2012)] as well as the intrusives found in the Farne group [NAM drilling report E06-01], constraining them to a Late Devonian to Early Carboniferous age. The southern seismic line of this study does not show reflectors at the same stratigraphic levels (Figure 11, bottom panel) so the extent of the volcanics may have been limited. There are no drillings for the lithologies under the Kyle limestone in the study area, so the composition remains unknown and thus the interpretation cannot be confirmed.

Thrusts may also explain the tilted reflectors with high amplitudes under the Kyle limestone west of the SG. Phillips et al. (2016) found reactivated Caledonian thrusts with a comparable seismic signal (Figures 9 and 10, bottom panels). Expected syn-kinematic patterns related to fault activity are not observed however. Often structures are not well preserved at these depths [Jeroen Smit, personal communication], making the interpretation more unlikely. Magnetic and Bouguer anomalies at the corresponding traces (Figures 15 and 16, bottom panels) suggest the presence of volcanics. A possibility could be that intrusion of volcanics masks the seismic signal of the expected syn-kinematic facies. The presence of thrust faults would explain the presence of pathways into more shallow levels however. The geometry of the reflectors is hard to ignore too, showing the transition the backside of the thrust to the depocenter of the footwall syncline. The vergence of the thrusts also agrees with the compressive tectonics during the Caledonian Orogeny [Ziegler (1990a)]. This research proposes the presence of both volcanics and remanant Caledonian thrust structures on the margin of Avalonia.

The lateral change in seismic facies of the Paleozoic units (Figures 9, 10 and 11, bottom panels) is likely the result different tectonic terranes (Figure 3) constituting the study area. The central part of the sections shows chaotic seismic facies, attributed to deformation during the Caledonian Orogeny and subsequent reactivation. Intrusions may also exert an influence on the seismic facies observed in the central parts of the sections. East and west of the CG different seismic facies can be explained by a change in lithology due to sediments being sourced from different locations and/or different margin geometries of Avalonia and Baltica. Crustal profiles from previous studies (Figures 18 and 19) indicate that the upper crust of Baltica is located more shallow than the upper crust of Avalonia. Paleozoic seismic facies east of the CG is generally more chaotic than west of the SG at more shallow, which may indicate that the lower crust of Baltica is indeed observed at relatively shallow levels.

An increase in mass deficit towards the east is suggested by the stepwise decrease in the Bouguer anomalies for all sections towards the east (Figures 15, 16 and 17, bottom panels). An explanation for this increase in

mass deficit combined with positive magnetic anomalies towards the east may be increasing thickness of the crystalline Baltic crust as shown by crustal profiles which extend further east by Lyngsie and Thybo (2007) and Smit et al. (2018) (Figures 18 and 19). Values indicated by the results of this research are equal in magnitude to those modelled for the Baltic crust from Figure 6 of Mazur et al. (2015). As the crust thickens, more dense mantle material is replaced, resulting in both negative Bouguer anomalies as well as positive magnetic anomalies due to the crystalline lithologies.

The combination of the spike at line A, the positive Bouguer anomaly in Figure 16 with the bright reflectors the Old Red group, which showing thickening, indicates that extension tectonics and volcanic activity were paired in the Late Devonian. The presence of high density intrusions causes the positive spike in the magnetic and the flattening of the Bouguer anomaly [Fowler et al. (1990)]. This agrees with the Late Devonian extension paired with volcanic activity [Lundmark et al. (2012)]. Other magnetic spikes are close to basement faults (Figures 15, 16, bottom panels). Instead of vertically intruding the Avalonian crust as proposed by the profile from Lyngsie and Thybo (2007) (Figure 18) the volcanics could have travelled up-slope along the detachment and rooted basement faults [Sleep (1997), Sleep (2006)]. Line A in Figure 15 and line B in Figure 10 show positive magnetic anomalies paired with Bouguer anomaly flats, suggesting volcanics are present at these locations too. The thick Baltic crust to the east may mute the expected positive Bouguer anomalies under the rift and produce flats instead.

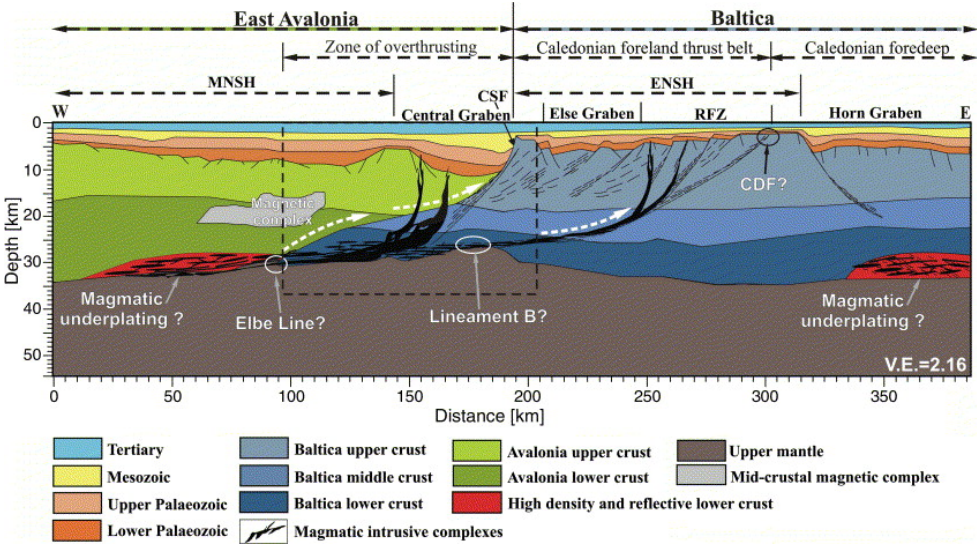


Figure 18: Crustal model along the MONA LISA 3 profile obtained from gravity and magnetic modelling by Lyngsie and Thybo (2007). Source: Lyngsie and Thybo (2007)

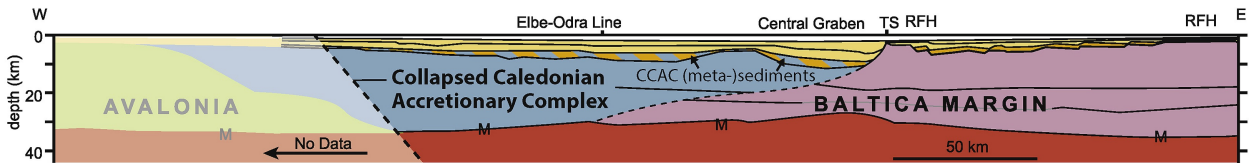


Figure 19: Interpretation based on seismic refraction profiles for the MONA LISA 3 profile [Smit et al. (2016)]. Moho (M), Thor Suture Zone (TS). Source: Smit et al. (2018).

The segment between lines 1 and 2 for Figures 15, 16 and 17 marks the rough extent of the rift system. The increase in sediment thickness, replacing dense crustal material, results in the decrease of the Bouguer anomaly. The extents are not the same for all the profiles however, which may be caused by an uneven distribution of volcanics. This is uncertain however, because there are no boreholes to confirm this explanation. The decrease in Bouguer anomaly east of line 2 in Figure 15 can be explained by the seismic line intersecting a large jump in the thickness of the CG (see Figure 6). An increase in the thickness of the Paleozoic and Mesozoic sedimentary thickness may yield this negative gradient of the Bouguer anomaly [Fowler et al. (1990)].

The interpreted seismic sections (Figures 9, 10 and 11, bottom panels) suggest that the Paleozoic basement consists out of different tectonic terranes on both sides of the CG. Besides lateral changes in seismic facies, various structures support this interpretation. An unconformity for Lower Paleozoic units under the CG is observed (Figures 9 and 10, bottom panels), with reflectors on both sides of the unconformity showing different orientations. Basement faults cut the Paleozoic units and root in this unconformity. When converted to absolute depth the geometries of these faults, as interpreted in the time domain, remain plausible. When the seismic lines are overlain on a map showing the extents of the different tectonic terranes of the study area (Figure 6) from Smit et al. (2018), the lines intersect the boundary between the remnant accretionary wedge of the Caledonian orogen and the margin of Baltica. The observed unconformity is thus interpreted as the detachment between Avalonia and Baltica which formed as a result of Baltica underthrusting Avalonia during the Caledonian Orogeny. An earlier used analogue for the situation observed for the CG is the Rhodope core complex which separates the hanging wall and the footwall observed in Greece [Smit et al. (2016)], which is assumed to result from extension due to gravitational collapse [Kydonakis et al. (2015)]. In this research the accretionary complex from the Caledonian Orogeny separates Baltica from Avalonia.

Extensive fault activity of Avalonia is suggested by fault blocks and thickness changes for the Farne group in the northern lines (Figures 9 and 10, bottom panels) and for the Limburg group in the southern line (Figure 11, bottom panel). This area was already weakened by the Caledonian Orogeny, explaining why extension occurred here [Beniest et al. (2018)]. Based on these observations the extension would have occurred during the Early Carboniferous for the northern line, shifting to the south during the Late Carboniferous. It is likely this is the extension event which started in the Late Devonian, indicated by volcanics found in well A17-01 [Lundmark et al. (2012)] and continued in the Early Carboniferous [Smit et al. (2018)]. Volcanics drilled around the ESP and this extension are thus diachronous and thus likely related. The decreasing Bouguer anomalies and increasing magnetic anomalies towards the west of each section (Figures 15, 16 and 17, bottom panels) suggests that a volcanic body may be present west of the study area. In the crustal profile of Lyngsie and Thybo (2007) magmatic underplating of Avalonia may coincide with this volcanic body. Volcanics observed in the study area may have been sourced from this magmatic underplating. Extensional faults may have acted as pathways for these volcanics to intrude the crust. This idea was also proposed by Lundmark et al. (2012) for Late Devonian volcanics and may have thus continued in the Early and Late Carboniferous.

## 5.2 Rifting style of the CG

The basement faults were likely preferentially reactivated as they were orthogonal to the direction of extension [Fossen (2016)]. It is unclear where these faults nucleated and how they propagated. Either they initiated at depth in the detachment and propagated upward or they initiated at shallow levels and rooted in the detachment. It is unlikely that antithetic faults nucleated from the underlying structure with opposed kinematics. Thus for the antithetic faults nucleation at shallow levels is favoured. It is likely that the synthetic faults were active as thrust faults during the Caledonian Orogeny, making it more likely that they nucleated at the detachment and propagated upward.

Strain localisation of extensional tectonics was already occurring in the Paleozoic. This is suggested by the half-graben structures observed when the sections are flattened on the Base Zechstein (Figures 12, 13 and 14, bottom panels). During later tectonic events the faults did not cut to more shallow levels due to the Zechstein deforming in a ductile way, absorbing the deformation. The process of pre-existing structures governing deformation during subsequent tectonic events seems to have repeated during the formation of the CG in the Mesozoic. Due to the Zechstein salt inhibiting further upward propagation, there are no faults in the Mesozoic sequence. The observed jumps, folding and tilting in the Mesozoic deposits being consistent with the locations and kinematics of basement faults (Figures 9, 10 and 11, bottom panels) suggest that, although not mechanically linked, these faults exerted a first-order control on the development of the CG. This is an interpretation consistent with other studies [e.g. Stewart et al. (1997), Erratt (1993), Phillips et al. (2016)]. Tilting and folding of supra-salt deposits in response to basement faulting has been shown to occur in the NS and other salt-influenced extensional domains [e.g. Stewart (2007), Bodego et al. (2018), Jackson et al. (2019), Phillips et al. (2019)]. The lack of faults and kinematic coherence of the Mesozoic cover with the basement faults suggest a soft-linked style of rifting for the CG. Figure 6 in Ferrer et al. (2017) shows results of analogue lab experiments on the influence of sub-salt structures on supra-salt basin development. The setup of this experiment are similar to the situation of the CG (pre-existing basement structure, presence of a ductile layer separating cover and basement and syn-kinematic deposition of the cover) and yield results similar to the structure of the CG. Basement faults accommodate the extensional motion and the salt absorbs the deformation, causing folding and tilting of the syn-kinematic basin infill.

The asymmetry observed when the Base Cretaceous Chalk is flattened (Figures 12, 13 and 14, middle panels) with the thickness of the Mesozoic increasing to the east indicates that after widespread extension in the Paleozoic extension focussed more towards the east, a mechanism where first a wide rift forms, followed by a more narrow rift [Beniest et al. (2018)]. Phillips et al. (2016) find that previously reactivated structures are already weakened and are thus more prone to further reactivation, a mechanism that may explain the shift of extension towards the detachment. Through this mechanism the detachment was able to accommodate a large part of the extension, explaining the deepest part of the CG being observed over the margin of Baltica (Figure 6). During the Late Triassic both the SG and CG were subsiding, but in the Jurassic the CG became the focus of extension due to



preferential reactivation of the faults above the detachment [Meyer et al. (2002)]. The absence of Triassic and Jurassic sediments west of the SG suggests that these areas were uplifted as a result of tilting due to Avalonia sliding off of the margin of Baltica.

The rifting model of the CG from van Winden et al. (2018) accounts for the basement faults. The geometries of the underlying Paleozoic units are not taken into account however. This results in an underestimation of the total amount of extension [Gibbs (1983)]. The deeper continuation of these faults in relation to the detachment is not given either. These details lack in the reconstruction, making it incomplete.

### **5.3 The influence of deep structure on the development of rifts**

Various models exist for the development of continental rifts [McKenzie (1978), Wernicke (1981), Barbier et al. (1986)]. The predicted geometry from the model of Wernicke (1981) gives an asymmetric basin where basement faults root in the detachment and a geometry somewhat representative of the CG, the other models yield geometries which do not represent the CG. The models lack important details however, such as the presence of a ductile layer in the crust, the presence of pre-existing basement structures or the occurrence of multiple tectonic events. The predicted fault geometries are evenly spaced and parallel to each other. The structural style of the entire crust being homogeneous. These predictions do not match the observations for the CG of this study however. Explanations for the differences between the predictions these models make and the observed structures is the lack of complexity of these models. Some important features these models do not account for studied in this research include crustal heterogeneity and reactivation of pre-existing basement structures. The results of this study, as well as previous studies [e.g. Braun and Beaumont (1987), Dunbar and Sawyer (1989), Van Wijhe (1987), Manatschal et al. (2015), Phillips et al. (2016), Beniest et al. (2018)], show that these factors are of major importance during subsequent basin development. This implies that in order to predict more plausible structures, the influence of pre-existing structures as well as multiple tectonic events have to be accounted for.

Various studies suggested the importance of these Paleozoic basement structures on the development of the CG [e.g. Ziegler (1990b), Coward (1993), Salazar-Mora et al. (2018)]. The results of this research indicate that the CG was formed due to extension being accommodated along basement faults and the detachment of Avalonia and Baltica and thus agree with these previous studies. In contrast, some other rifting models of the CG where suggest halokinesis as a first-order mechanism controlling the development of the CG [Hodgson et al. (1992)]. The location of basement faults seems to control the location of salt structures at the margins instead of the other way around. These findings agree with ter Borgh et al. (2019). This would suggest that halokinesis is of second-order importance to the basin formation. Salt structures may have had an important role, but this research finds that this is not of first-order importance.

## 6 Conclusions

In this research the first seismic interpretations of the Paleozoic stratigraphy and structures under the CG are presented. An attempt is made to construct a crustal model as well as to find a relation between basement faulting and the geometry of the overlying CG. Based on our results it can be concluded:

- Well data combined with the magnetic and Bouguer anomalies suggest that extensive tectonics in Avalonia during the Late Devonian to the Late Carboniferous was paired with volcanic activity.
- South of the ESP thrust structures from the Caledonian Orogeny, later reactivated, may be present in the Avalonian crust. These faults may have acted as pathways for volcanic intrusions.
- Seismic sections can be used to further constrain the locations of various tectonic terranes involved in the NS rift system. Lateral changes in facies indicate the locations of Avalonia, the collapsed accretionary complex and Baltica.
- Pre-existing basement structures are of major importance in subsequent basin development. The detachment between Avalonia and Baltica allowed for the localisation of strain, resulting in the formation of Paleozoic basement faults. The formation of the CG was driven by displacement along these basement faults. This means that the pre-existing crustal structure was of significant importance during the development of the CG.
- Rifting was more widespread over the entire area in the Paleozoic, followed by the SG and CG subsiding. Especially in the Jurassic extension focused directly above the detachment at the CG.
- The asymmetry of the CG is a result of asymmetric extension. Simple models fail to predict the geometry of a salt-influenced polyphase rift. In order to predict more plausible results, various factors such as the presence of salt, pre-existing structures or polyphase rifting have to be incorporated in rift models.

This research stresses the importance of inheritance of basement structures on subsequent basin development, shown by a case study of the CG. During subsequent tectonic events strain was further localised on pre-existing structures in the NS.

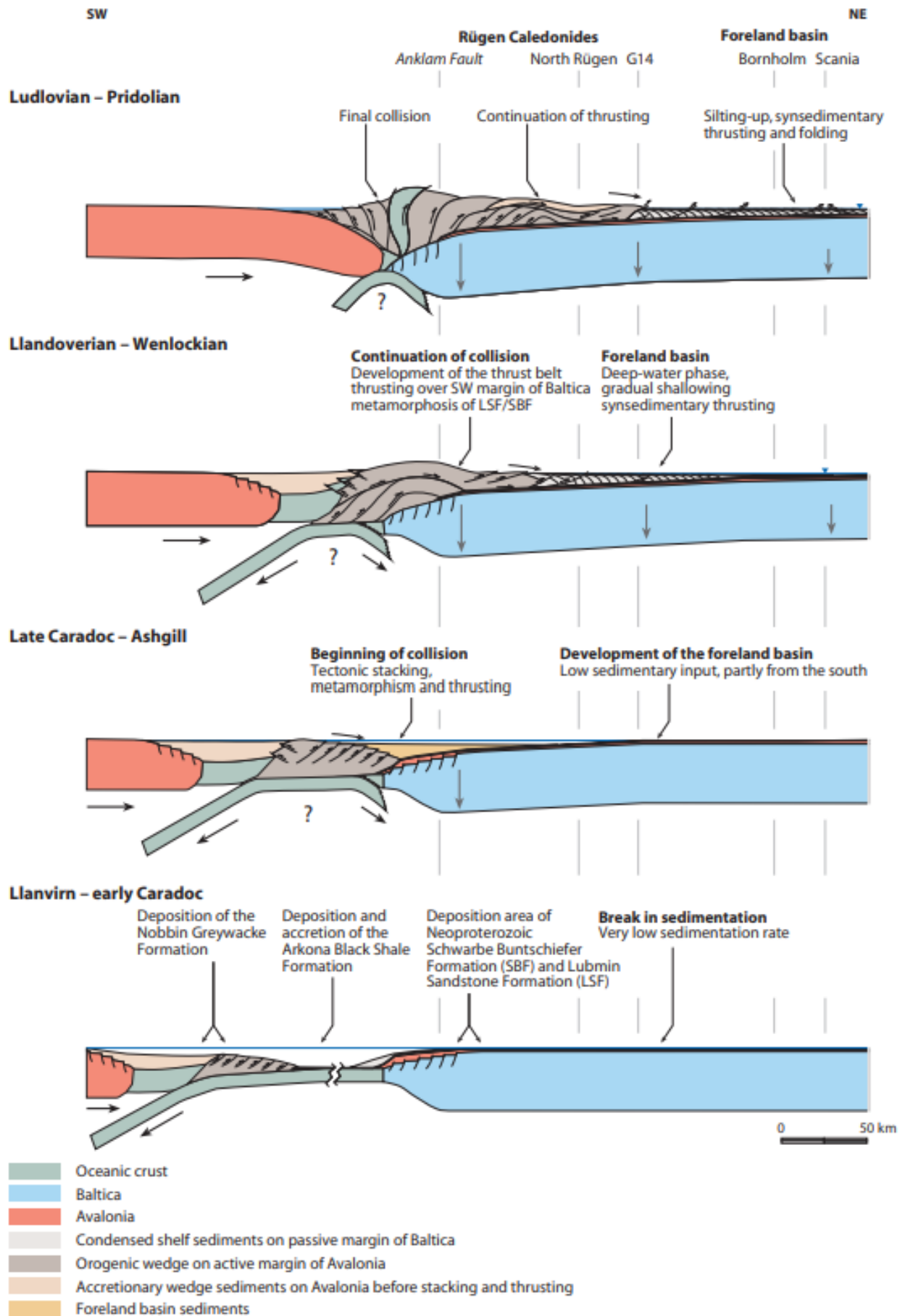











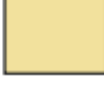
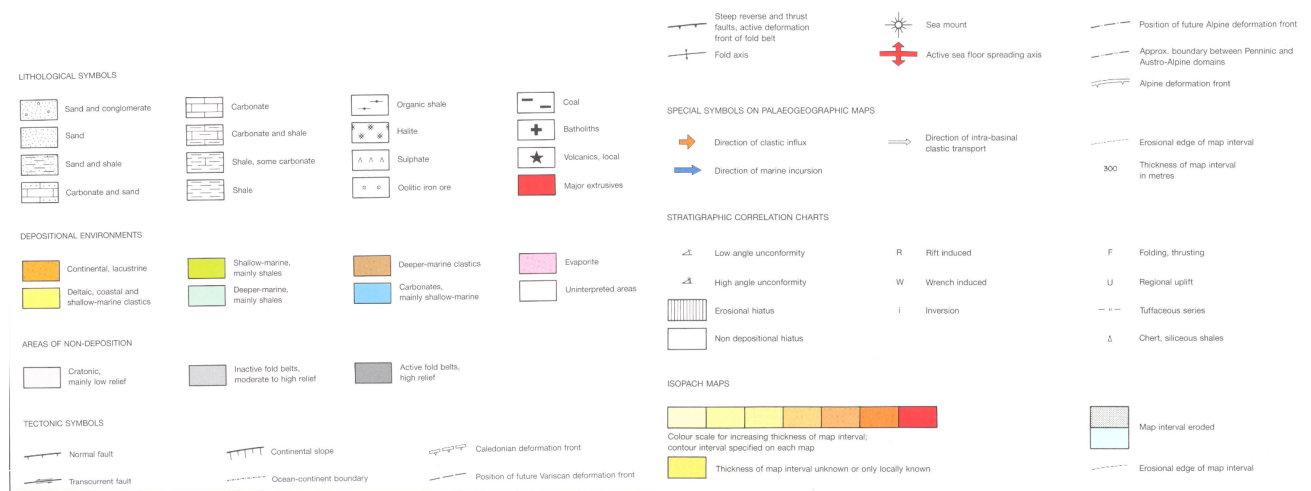


Figure 20: This figure shows the different processes which occurred during the collision between Avalonia and Baltica, occurring in the Silurian. Thrusts develop between between Avalonia and Baltica. Some foreland thrusts may reach relatively far on to Baltica. Source: Doornenbal and Stevenson (2010).

## 7 Appendix

Lithological unit	Colour
NS Supergroup	
Cretaceous chalk	
Rijnland group	
Schieland group	
Altena group	
Upper Germanic Trias	
Lower Germanic Trias	
Zechstein	
Limburg group	
Farne group	
Old Red group	
Kyle limestone	

This legend shows the color code for the stratigraphic units used in the line drawings and depth converted sections shown in this research.



These figures show the legend for Figure 4. Source: Ziegler (1990a)

## Bibliography

- T. Abramovitz, A. Berthelsen, and F. Schjoth. Mona lisa-deep seismic investigations of the lithosphere in the southeastern north sea. *Oceanographic Literature Review*, 11(44):1287, 1997.
- M. Ballèvre, V. Bosse, C. Ducassou, and P. Pitra. Palaeozoic history of the armorican massif: models for the tectonic evolution of the suture zones. *Comptes Rendus Geoscience*, 341(2-3):174–201, 2009.
- F. Barbier, J. Duvergé, and X. Le Pichon. Structure profonde de la marge nord-gascogne. implications sur le mécanisme de rifting et de formation de la marge continentale. *Bulletin des centres de recherches exploration-Production Elf-Aquitaine*, 10(1):105–121, 1986.
- A. Beniést, E. Willingshofer, D. Sokoutis, and W. Sassi. Extending continental lithosphere with lateral strength variations: effects on deformation localization and margin geometries. *Frontiers in Earth Science*, 6:148, 2018.
- A. Berthelsen. Tectonic evolution of europe. from precambrian to variscan europe. In *A Continent Revealed, the European Geotravers*, pages 153–164. 1992.
- S. Bland, P. Griffiths, and D. Hodge. Restoring the seismic image with a geological rule base. *first break*, 22(4), 2004.
- A. Bodego, E. Iriarte, M. López-Horgue, and I. Álvarez. Rift-margin extensional forced folds and salt tectonics in the eastern basque-cantabrian rift basin (western pyrenees). *Marine and Petroleum Geology*, 91:667–682, 2018.
- R. Bouroullec, R. Verreussel, C. Geel, G. de Bruin, M. Zijp, D. Kőrösi, D. Munsterman, N. Janssen, and S. Kerstholt-Boegehold. Tectonostratigraphy of a rift basin affected by salt tectonics: synrift middle jurassic–lower cretaceous dutch central graben, terschelling basin and neighbouring platforms, dutch offshore. *Geological Society, London, Special Publications*, 469(1):269–303, 2018.
- J. Braun and C. Beaumont. Styles of continental rifting: results from dynamic models of lithospheric extension. 1987.
- J. Clark, S. Stewart, and J. Cartwright. Evolution of the nw margin of the north permian basin, uk north sea. *Journal of the Geological Society*, 155(4):663–676, 1998.
- L. Cocks and R. Fortey. Avalonia: a long-lived terrane in the lower palaeozoic? *Geological Society, London, Special Publications*, 325(1):141–155, 2009.
- C. Cornford and J. Brooks. Tectonic controls on oil and gas occurrences in the north sea area: Chapter 34: North sea and barents shelf. 1989.
- M. Coward. The effect of late caledonian and variscan continental escape tectonics on basement structure, paleozoic basin kinematics and subsequent mesozoic basin development in nw europe. In *Geological Society, London, Petroleum Geology Conference series*, volume 4, pages 1095–1108. Geological Society of London, 1993.

- M. Coward. Structural and tectonic setting of the permo-triassic basins of northwest europe. *Geological Society, London, Special Publications*, 91(1):7–39, 1995.
- M. Coward, J. Dewey, M. Hempton, and J. Holroyd. Tectonic evolution. *The Millennium Atlas: Petroleum Geology of the Central and Northern North Sea. Geological Society, London*, 17:33, 2003.
- J. De Jager. Inverted basins in the netherlands, similarities and differences. *Netherlands Journal of Geosciences*, 82(4):339–349, 2003.
- C. H. Dix. Seismic velocities from surface measurements. *Geophysics*, 20(1):68–86, 1955.
- H. Doornenbal and A. Stevenson. *Petroleum geological atlas of the Southern Permian Basin area*. EAGE, 2010.
- A. Dronkers and F. Mrozek. Inverted basins of the netherlands. *First Break*, 9(9):409–425, 1991.
- O. B. Duffy, R. E. Bell, C. A.-L. Jackson, R. L. Gawthorpe, and P. S. Whipp. Fault growth and interactions in a multiphase rift fault network: Horda platform, norwegian north sea. *Journal of Structural Geology*, 80: 99–119, 2015.
- J. A. Dunbar and D. S. Sawyer. How preexisting weaknesses control the style of continental breakup. *Journal of Geophysical Research: Solid Earth*, 94(B6):7278–7292, 1989.
- D. Erratt. Relationships between basement faulting, salt withdrawal and late jurassic rifting, uk central north sea. In *Geological Society, London, Petroleum Geology Conference series*, volume 4, pages 1211–1219. Geological Society of London, 1993.
- R. Færseth. Interaction of permo-triassic and jurassic extensional fault-blocks during the development of the northern north sea. *Journal of the Geological Society*, 153(6):931–944, 1996.
- R. A. Fattah, J. Verweij, N. Witmans, and J. Ten Veen. Reconstruction of burial history, temperature, source rock maturity and hydrocarbon generation in the northwestern dutch offshore. *Netherlands Journal of Geosciences*, 91(4):535–554, 2012.
- O. Ferrer, K. McClay, and N. Sellier. Influence of fault geometries and mechanical anisotropies on the growth and inversion of hanging-wall synclinal basins: insights from sandbox models and natural examples. *Geological Society, London, Special Publications*, 439(1):487–509, 2017.
- H. Fossen. *Structural geology*. Cambridge University Press, 2016.
- C. M. R. Fowler, C. M. R. Fowler, and M. Fowler. *The solid earth: an introduction to global geophysics*. Cambridge University Press, 1990.
- R. Frost. The evolution of the viking graben tilted fault block structures: a compressional origin. In *Conference on petroleum geology of North West Europe. 3*, pages 1009–1024, 1987.

- A. Gibbs. Balanced cross-section construction from seismic sections in areas of extensional tectonics. *Journal of structural geology*, 5(2):153–160, 1983.
- A. Gibbs. Deep seismic profiles in the northern north sea. In *Conference on petroleum geology of North West Europe*. 3, pages 1025–1028, 1987.
- K. W. Glennie. Introduction to the petroleum geology of the north sea. 1984.
- M. B. Gowers and A. Sæbøe. On the structural evolution of the central trough in the norwegian and danish sectors of the north sea. *Marine and Petroleum Geology*, 2(4):298–318, 1985.
- P. Heybroek et al. On the structure of the dutch part of the central north sea graben. 1975.
- N. Hodgson, J. Farnsworth, and A. Fraser. Salt-related tectonics, sedimentation and hydrocarbon plays in the central graben, north sea, ukcs. *Geological Society, London, Special Publications*, 67(1):31–63, 1992.
- T. Husmo, G. Hamar, O. Høiland, E. Johannessen, A. Rømuld, A. Spencer, R. Titterton, D. Evans, C. Graham, A. Armour, et al. Lower and middle jurassic. *The Millennium Atlas: Petroleum Geology of the Central and Northern North Sea*. Geological Society, London, 129:156, 2003.
- C. A.-L. Jackson and M. M. Lewis. Structural style and evolution of a salt-influenced rift basin margin; the impact of variations in salt composition and the role of polyphase extension. *Basin Research*, 28(1):81–102, 2016.
- C. A.-L. Jackson, G. M. Elliott, E. Royce-Rogers, R. L. Gawthorpe, and T. E. Aas. Salt thickness and composition influence rift structural style, northern north sea, offshore norway. *Basin Research*, 31(3):514–538, 2019.
- M. Jackson and B. Vendeville. Regional extension as a geologic trigger for diapirism. *Geological society of America bulletin*, 106(1):57–73, 1994.
- S. F. Jamaludin, A. A. Latiff, and D. Ghosh. Structural balancing vs horizon flattening on seismic data: example from extensional tectonic setting. In *IOP Conference Series: Earth and Environmental Science*, volume 23, page 012003. IOP Publishing, 2015.
- S. Jansen, W. Bradbury, B. E. Kjølhamar, et al. Clari-fi™ broadband processed 2d seismic in portugal and the mid-north sea high. 2016.
- J. F. Karlo, F. S. van Buchem, J. Moen, and K. Milroy. Triassic-age salt tectonics of the central north sea. *Interpretation*, 2(4):SM19–SM28, 2014.
- K. Kydonakis, J.-P. Brun, and D. Sokoutis. North aegean core complexes, the gravity spreading of a thrust wedge. *Journal of Geophysical Research: Solid Earth*, 120(1):595–616, 2015.



- R. Littke, U. Bayer, D. Gajewski, and S. Nelskamp. *Dynamics of complex intracontinental basins: the central European basin system*. Springer Science & Business Media, 2008.
- G. Lott, T. Wong, M. Duser, J. Andsbjerg, E. Mönnig, A. Feldman-Olszewska, and R. Verreussel. Jurassic. *Petroleum Geological Atlas of the Southern Permian Basin Area*. European Association of Geoscientists and Engineers (EAGE), Houten, The Netherlands, 175:193, 2010.
- A. Lundmark, R. Gabrielsen, H. Austrheim, K. Flaath, T. Strand, and S. Ohm. Late devonian rifting in the central north sea: Evidence from altered felsic volcanic rocks in the embla oil field. *Marine and Petroleum Geology*, 29(1):204–218, 2012.
- S. B. Lyngsie and H. Thybo. A new tectonic model for the laurentia- avalonia- baltica sutures in the north sea: A case study along mona lisa profile 3. *Tectonophysics*, 429(3-4):201–227, 2007.
- G. Manatschal, L. Lavier, and P. Chenin. The role of inheritance in structuring hyperextended rift systems: Some considerations based on observations and numerical modeling. *Gondwana Research*, 27(1):140–164, 2015.
- K. J. Matthews, K. T. Maloney, S. Zahirovic, S. E. Williams, M. Seton, and R. D. Mueller. Global plate boundary evolution and kinematics since the late paleozoic. *Global and Planetary Change*, 146:226–250, 2016.
- S. Mazur, M. Mikolajczak, P. Krzywiec, M. Malinowski, V. Buffenmyer, and M. Lewandowski. Is the teisseyre-tornquist zone an ancient plate boundary of baltica? *Tectonics*, 34(12):2465–2477, 2015.
- S. Mazur, S. J. Porebski, A. Kedzior, M. Paszkowski, T. Podhalańska, and P. Poprawa. Refined timing and kinematics for baltica–avalonia convergence based on the sedimentary record of a foreland basin. *Terra Nova*, 30(1):8–16, 2018.
- D. McKenzie. Some remarks on the development of sedimentary basins. *Earth and Planetary science letters*, 40(1):25–32, 1978.
- V. Meyer, A. Nicol, C. Childs, J. Walsh, and J. Watterson. Progressive localisation of strain during the evolution of a normal fault population. *Journal of Structural Geology*, 24(8):1215–1231, 2002.
- D. Mishra. Gravity and magnetic methods for geological studies. *Hyderabad: BS Publications*, 2011.
- D. Munsterman, R. Verreussel, H. Mijlief, N. Witmans, S. Kerstholt-Boegehold, and O. Abbink. Revision and update of the callovian-ryazanian stratigraphic nomenclature in the northern dutch offshore, ie central graben subgroup and scruff group. *Netherlands Journal of Geosciences*, 91(4):555–590, 2012.
- T. Nalpas, S. Le Douaran, J.-P. Brun, P. Unternehr, and J.-P. Richert. Inversion of the broad fourteens basin (offshore netherlands), a small-scale model investigation. *Sedimentary Geology*, 95(3-4):237–250, 1995.

- E.-R. Neumann, M. Wilson, M. Heeremans, E. A. Spencer, K. Obst, M. J. Timmerman, and L. Kirstein. Carboniferous-permian rifting and magmatism in southern scandinavia, the north sea and northern germany: a review. *Geological Society, London, Special Publications*, 223(1):11–40, 2004.
- T. Pharaoh, M. Dusaar, M. Geluk, F. Kockel, C. Krawczyk, P. Krzywiec, M. Scheck-Wenderoth, H. Thybo, O. Vejbæk, and J. D. Van Wees. Tectonic evolution. In *Petroleum geological atlas of the Southern Permian Basin area*, pages 25–57. EAGE Publications bv (Houten), 2010.
- T. B. Phillips, C. A. Jackson, R. E. Bell, O. B. Duffy, and H. Fossen. Reactivation of intrabasement structures during rifting: A case study from offshore southern norway. *Journal of Structural Geology*, 91:54–73, 2016.
- T. B. Phillips, H. Fazlikhani, R. L. Gawthorpe, H. Fossen, C. A.-L. Jackson, R. E. Bell, J. I. Faleide, and A. Rotevatn. The influence of structural inheritance and multiphase extension on rift development, the northern north sea. *Tectonics*, 2019.
- G. Pieńkowski, M. E. Schudack, P. Bosák, R. Enay, A. Feldman-Olszewska, J. Golonka, J. Gutowski, G. F. Herngreen, P. Jordan, M. Krobicki, et al. Jurassic. *Geology of Central Europe*, 6(2):823–922, 2008.
- R. Rattey and A. Hayward. Sequence stratigraphy of a failed rift system: the middle jurassic to early cretaceous basin evolution of the central and northern north sea. In *Geological Society, London, Petroleum Geology Conference series*, volume 4, pages 215–249. Geological Society of London, 1993.
- P. Rawson and L. Riley. Latest jurassic-early cretaceous events and the “late cimmerician unconformity” in north sea area. *AAPG Bulletin*, 66(12):2628–2648, 1982.
- G. Remmelts. Fault-related salt tectonics in the southern north sea, the netherlands. 1995.
- E. Robein. *Velocities, time-imaging, and depth-imaging in reflection seismics: principles and methods*. EAGE publications, 2003.
- C. A. Salazar-Mora, R. S. Huismans, H. Fossen, and M. Egydio-Silva. The wilson cycle and effects of tectonic structural inheritance on rifted passive margin formation. *Tectonics*, 37(9):3085–3101, 2018.
- N. H. Sleep. Lateral flow and ponding of starting plume material. *Journal of Geophysical Research: Solid Earth*, 102(B5):10001–10012, 1997.
- N. H. Sleep. Mantle plumes from top to bottom. *Earth-Science Reviews*, 77(4):231–271, 2006.
- J. Smit, J.-D. van Wees, and S. Cloetingh. The thor suture zone: From subduction to intraplate basin setting. *Geology*, 44(9):707–710, 2016.
- J. Smit, J.-D. van Wees, and S. Cloetingh. Early carboniferous extension in east avalonia: 350 my record of lithospheric memory. *Marine and Petroleum Geology*, 92:1010–1027, 2018.

- S. Stewart. Salt tectonics in the north sea basin: a structural style template for seismic interpreters. *Special Publication-Geological Society of London*, 272:361, 2007.
- S. Stewart, A. Ruffell, and M. Harvey. Relationship between basement-linked and gravity-driven fault systems in the ukcs salt basins. *Marine and Petroleum Geology*, 14(5):581–604, 1997.
- M. ter Borgh, B. Jaarsma, and E. Rosendaal. Structural development of the northern dutch offshore: Paleozoic to present. *Geological Society, London, Special Publications*, 471(1):115–131, 2019.
- T. H. Torsvik and L. R. M. Cocks. Gondwana from top to base in space and time. *Gondwana Research*, 24(3-4): 999–1030, 2013.
- T. H. Torsvik and E. F. Rehnström. The tornquist sea and baltica–avalonia docking. *Tectonophysics*, 362(1-4): 67–82, 2003.
- T. H. Torsvik, D. Carlos, J. Mosar, L. R. M. Cocks, and T. Malme. Global reconstructions and north atlantic paleogeography 440 ma to recent. *BATLAS–Mid Norway plate reconstruction atlas with global and Atlantic perspectives. Geological Survey of Norway, Trondheim*, 18:39, 2002.
- T. H. Torsvik, M. A. Smethurst, K. Burke, and B. Steinberger. Long term stability in deep mantle structure: Evidence from the ~ 300 ma skagerrak-centered large igneous province (the sclip). *Earth and Planetary Science Letters*, 267(3-4):444–452, 2008.
- J. R. Underhill and M. Partington. Jurassic thermal doming and deflation in the north sea: implications of the sequence stratigraphic evidence. In *Geological Society, London, Petroleum Geology Conference series*, volume 4, pages 337–345. Geological Society of London, 1993.
- W. Van Dalssen, J. Doornenbal, S. Dortland, and J. Gunnink. A comprehensive seismic velocity model for the netherlands based on lithostratigraphic layers. *Netherlands Journal of Geosciences*, 85(4):277–292, 2006.
- J.-D. Van Wees, R. Stephenson, P. Ziegler, U. Bayer, T. McCann, R. Dadlez, R. Gaupp, M. Narkiewicz, F. Bitzer, and M. Scheck. On the origin of the southern permian basin, central europe. *Marine and Petroleum Geology*, 17(1):43–59, 2000.
- D. v. Van Wijhe. Structural evolution of inverted basins in the dutch offshore. *Tectonophysics*, 137(1-4):171–219, 1987.
- M. van Winden, J. de Jager, B. Jaarsma, and R. Bouroullec. New insights into salt tectonics in the northern dutch offshore: a framework for hydrocarbon exploration. *Geological Society, London, Special Publications*, 469(1):99–117, 2018.
- O. Vejbæk and C. Andersen. Post mid-cretaceous inversion tectonics in the danish central graben–regionally synchronous tectonic events. *Bulletin of the Geological Society of Denmark*, 49(2):93–204, 2002.

- J. Verniers, T. Pharaoh, L. André, T. Debacker, W. De Vos, M. Everaerts, A. Herbosch, J. Samuelsson, M. Sintubin, and M. Vecoli. The cambrian to mid devonian basin development and deformation history of eastern avalonia, east of the midlands microcraton: new data and a review. *Geological Society, London, Special Publications*, 201(1):47–93, 2002.
- R. Verreussel, R. Bouroulllec, D. Munsterman, K. Dybkjær, C. Geel, A. Houben, P. Johannessen, and S. Kerstholt-Boegehold. Stepwise basin evolution of the middle jurassic–early cretaceous rift phase in the central graben area of denmark, germany and the netherlands. *Geological Society, London, Special Publications*, 469(1): 305–340, 2018.
- J. Verweij, M. Souto Carneiro Echternach, and N. Witmans. Terschelling basin and southern dutch central graben burial history, temperature, source rock maturity and hydrocarbon generation-area 2a. *Built Environment and Geosciences–National Geological Survey, Utrecht, Netherlands, TNO report TNO-034-UT-2009-02065/A*, 2009.
- B. Wernicke. Insights from basin and range surface geology for the process of large-scale divergence of the continental lithosphere. In *Processes of Planetary Rifting*, volume 457, page 90, 1981.
- J. A. Winchester, T. C. Pharaoh, and J. Verniers. Palaeozoic amalgamation of central europe: an introduction and synthesis of new results from recent geological and geophysical investigations. *Geological Society, London, Special Publications*, 201(1):1–18, 2002.
- T. Wong, D. Batjes, and J. de Jager. Geological development. in: *Geology of the netherlands*. royal netherlands academy of arts and sciences, amsterdam. pages 5–26, 01 2007.
- N. Woodcock. Ordovician volcanism and sedimentation on eastern avalonia. *Geological History of Britain and Ireland*, pages 162–176, 2012.
- P. Ziegler. Faulting and graben formation in western and central europe. *Philosophical Transactions of the Royal Society of London. Series A, Mathematical and Physical Sciences*, 305(1489):113–143, 1982a.
- P. Ziegler. Triassic rifts and facies patterns in western and central europe. *Geologische Rundschau*, 71(3):747–772, 1982b.
- P. Ziegler. Tectonic and palaeogeographic development of the north sea rift system. In *Tectonic evolution of the North Sea rifts*, volume 81, pages 1–36. Oxford Science Publications Oxford, 1990a.
- P. Ziegler. North sea rift system. *Tectonophysics*, 208(1-3):55–75, 1992.
- P. A. Ziegler. Evolution of the arctic-north atlantic and the western tethys: A visual presentation of a series of paleogeographic-paleotectonic maps. *AAPG memoir*, 43:164–196, 1988.
- P. A. Ziegler. *Geological atlas of Western and Central Europe.[Hauptbd.](1990)*. Shell Internat. Petroleum Maatschappij, 1990b.

P. A. Ziegler. *Evolution of Laurussia: A study in Late Palaeozoic plate tectonics*. Springer Science & Business Media, 2012.